ANKARA YILDIRIM BEYAZIT UNIVERSITY

GRADUATE SCHOOL OF NATURAL AND APPLIED SCIENCES



HETEROJUNCTION PHOTODIODE FABRICATED FROM TiO_2 NANORODS DEPOSITED ON p-Si

M. Sc. Thesis by

Betül ŞEKERTEKİN

Department of Energy Systems Engineering

February, 2022

ANKARA

HETEROJUNCTION PHOTODIODE FABRICATED FROM TiO_2 NANORODS DEPOSITED ON p-Si

A Thesis Submitted to

The Graduate School of Natural and Applied Sciences of

Ankara Yıldırım Beyazıt University

In Partial Fulfillment of the Requirements for the Degree of

Master of Science in Department of Energy Systems Engineering

by

Betül ŞEKERTEKİN

February, 2022

ANKARA

M. Sc. THESIS EXAMINATION RESULT FORM

We have read the thesis entitled **"HETEROJUNCTION PHOTODIODE FABRICATED FROM TiO_2 NANORODS DEPOSITED ON p-Si"** completed by **Betül ŞEKERTEKİN** under the supervision of **Prof. Dr. Abdullah YILDIZ** and we certify that in our opinion it is fully adequate, in scope and in quality, as a thesis for the degree of Master of Science.

Prof. Dr. Abdullah YILDIZ

Supervisor

Prof. Dr. Bülent YEŞİLATA

Jury Member

Assoc. Prof. Dr. Yasemin ŞAFAK ASAR

Jury Member

Prof. Dr. Sadettin ORHAN

Director

Graduate School of Natural and Applied Sciences

ETHICAL DECLARATION

I hereby declare that, in this thesis, which has been prepared in accordance with the Thesis Writing Manual of Graduate School of Natural and Applied Sciences,

- All data, information, and documents were obtained in the framework of academic and ethical rules,
- All information, documents, and assessments are presented in accordance with scientific ethics and morals,
- All of the materials that have been utilized are fully cited and referenced,
- No changes have been made in the utilized materials,
- All of the work presented is original,

and in any contrary case of the above statements, I agree to renounce all of my legal rights.

Date: 10/02/2022 **Signature: ……..**

Name & Surname: Betül ŞEKERTEKİN

ACKNOWLEDGEMENTS

I would like to thank my supervisior Prof. Dr. Abdullah YILDIZ for dealing and believing in me throught this project. Him experience in the field and endless new ideas in both theoretical and practical parts were conclusive for the success of the work. Thank you for everything.

I would also like to thank Kenan ÖZEL and Abdullah ATILGAN for their guidance and effort. Their door always open, and their support much appreciated.

Finally, I must express my gratitude to my parents for encouraging and supporting me throughout my master education. Thank you.

2022, February 10 **Betül ŞEKERTEKİN**

For my father.

HETEROJUNCTION PHOTODIODE FABRICATED FROM TiO_2 NANORODS DEPOSITED ON p-Si

ABSTRACT

Heterojunction engineering of metal-oxide materials provides an exciting opportunity to fabricate novel optoelectronic devices. Titanium dioxide (TiO_2) is a promising candidate material for light detection. The objectives of this thesis are to prepare a *p-n* heterojunction photodiode using titanium dioxide (TiO_2) as an emitter layer based on n-TiO_2/p-Si structure. In this thesis, we assembled n-TiO_2 nanorods deposited on p-Si substrates via hydrothermal method to form a n-TiO_2/p-Si *p-n* heterojunction photodiode where photo-generated electrons travel from p-Si to n-TiO_2 over a barrier under illumination. The crystal structure, band gap energy and some important electrical parameters of the fabricated device have been excracted via X-Ray Diffraction, Scanning Electron Microscopy, UV-Vis Spectroscopy and Current-Voltage measurements. The results showed that the device is sensitive to ultraviolet light (365 nm). The fabricated photodiode showed excellent photosensitivity with a maximum photo responsivity of 1.41A/W, photosensitivity of 80, detectivity of $8.32x10^{11}$ Jones and a photoresponse time of 25 ms at 365 nm ultraviolet light.

Keywords: Heterojunction, TiO_2, Nanorods, Photodiode.

p-Si ALTTAŞ ÜZERİNE BÜYÜTÜLMÜŞ NANOÇUBUKLAR İLE HETEROEKLEM FOTODİYOT ÜRETİMİ

ÖZ

Metal oksit malzemelerin heterojunction mühendisliği, yeni optoelektronik cihazlar üretmek için heyecan verici bir fırsat sağlar. Titanyum dioksit (TiO_2), ışık deteksiyonu için umut verici bir aday malzemedir. Bu tezin amacı, n-TiO_2/p-Si yapısına dayalı olarak titanyum dioksit (TiO_2) emiter katman olarak kullanılarak bir p-n heteroeklemli fotodiyot hazırlamaktır. Bu tez çalışmasında, ışık altında üretilen elektronların bir bariyer üzerinden p-Si'den n-TiO_2'ye hareket ettiği bir n-TiO_2/p-Si p-n heteroeklemli fotodiyot oluşturmak için hidrotermal yöntemle p-Si alttaşlar üzerine n-TiO_2 nanoçubukları biriktirildi. Üretilen cihazın kristal yapısı, bant aralığı enerjisi ve bazı önemli elektriksel parametreleri, X-ışını kırınımı, taramalı elektron mikroskobu, UV-Vis spektroskopisi ve akım-voltaj ölçümleri yoluyla belirlendi. Sonuçlar, cihazın ultraviyole ışığa (365 nm) duyarlı olduğunu gösterdi. Üretilen fotodiyot, 1.41A/W maksimum foto-duyarlılığı, 80 foto-duyarlılığı, $8.32x10^{11}$ Jones ve 365 nm ultraviyole ışığında 25 ms foto-tepki süresi ile mükemmel foto-duyarlılık gösterdi.

Anahtar Kelimeler: Heteroeklemler, TiO_2, Nanoçubuklar, Fotodiyot.

CONTENTS

M. Sc. THESIS EXAMINATION RESULT FORM ii
ETHICAL DECLARATION iii
ACKNOWLEDGEMENTS iv
ABSTRACT v
ÖZ vi
CONTENTS vii
NOMENCLATURE ix
LIST OF TABLES xi
LIST OF FIGURES xii

CHAPTER 1 - INTRODUCTION 1
CHAPTER 2 - TiO_2 BASED P-N HETEROJUNCTION STRUCTURES 5
2.1 Material Properties of TiO_2 5
2.2 TiO_2/p-Si Heterojunction Structures 7
2.3 Working Principle of p-n junction-based Photodiodes 9
2.4 Evaluation of Photodiode Parameters 14
CHAPTER 3 - DEVICE FABRICATION 17
3.1 The Solution Preparation for TiO_2 Thin Film 17
3.2 Cleaning Processes for Glass and p-Si substrates 18
3.3 Deposition 20
3.4 Metallization 22
3.5 Characterizations 23
3.5.1 X-Ray Diffraction (XRD) Measurement 24
3.5.2 Scanning Electron Microscopy (SEM) measurement 25
3.5.3 UV-VIS-NIR Measurements 26
3.5.4 Current-Voltage (I-V) Measurements 26
3.5.5 The Time-Resolved Photoresponse (I-t) Measurements 28
CHAPTER 4 - RESULTS AND DISCUSSION 29
4.1 X-Ray Diffraction Results 29
4.2 Scanning Electron Microscopy (SEM) Results 30
4.3 UV-VIS-NIR Results 30
4.4 The Current-Voltage Results 31

4.5 The Time-Resolved Photoresponse (I-t) Results..... 33
CHAPTER 5 - CONCLUSIONS..... 35
REFERENCES..... 36

CURRICULUM VITAE..... 45

NOMENCLATURE

Symbols

2θ	Measured between incident beams that called Bragg angle
C_J	Junction capacitance
D^*	Detectivity
E_{field}	Internal electric field
EQE	External quantum efficiency
I_P	Photocurrent
I_{tn}	Total noise of photodiode
J_D	Dark current density
J_L	Light current density
LDR	Linear dynamic range
NEP	Noise equivalent power
P_{in}	Incident light power
PR	Photoresponsivity
PS	Photosensitivity
R_S	Series resistance
R_{sh}	Shunt resistance
R_λ	Responsivity
V_B	Barrier voltage
V_{bi}	Built in potential
λ	Wavelenght
τ_d	Decay time
τ_r	Rise time
Ω	Ohm

Acronyms

Ag	Silver
Au	Gold
DIW	Deiyonize water
EtOH	Ethanol
H_2O_2	Hydrogen Peroxide
H_2SO_4	Sulfuric Acid
HCI	Hydrochloric acid
HF	Hydrofluoric acid
HoAc	Acetic acid
mm	Mililiter
nm	Nanometer
NRs	Nanorods
SEM	Scanning Electron Microscopy
Si	Silicon
SiO_2	Silicon dioxide
TFT	Thin film transistors
Ti	Titanium
$TiCI_4$	Titanium IV Chloride
TiO_2	Titanium dioxide
TTIP	Titanium-IV Isopropoxide
UV	Ultraviolet
XRD	X-Ray Diffraction

LIST OF TABLES

Table 2.1 Properties of TiO_2 7

Table 3.1 The materials and quantities for second part of hydrothermal method 18

Table 4.1 Comparison of key parameters of reported metal-oxide based UV photodiodes 34

LIST OF FIGURES

Figure 2.1 Schematic structure of TiO_2 6

Figure 2.2 Energy band diagram of n-TiO_2/p-Si heterojunction (a) in the dark (b) under light 9

Figure 2.3 Different types of heterojunctions 10

Figure 2.4 Structure of the p-n junction diode 10

Figure 2.5 Band diagram of p-n junction 11

Figure 2.6 Band diagram of p-n junction diode under themal equilibrium 12

Figure 2.7 Band Diagram of p-n junction diode at forward bias 13

Figure 2.8 Band Diagram of p-n junction diode at reverse bias 14

Figure 2.9 The equivalent circuit of photodiode 14

Figure 2.10 The reverse bias characteristics of photodiode devices under dark and light conditions 15

Figure 3.1 The fundamental structure of the photodiode 17

Figure 3.2 Preparation of the solution for second part of hydrothermal deposition . 18

Figure 3.3 The cleaning process for p-Si substrates 19

Figure 3.4 UV/Ozone cabin 20

Figure 3.5 Glass and p-Si substrates located in solution 21

Figure 3.6 p-Si wafers in autoclave apparatus 21

Figure 3.7 Screen printing masks for rear side and front side respectively 22

Figure 3.8 Ag contacts on front side after metallization process 23

Figure 3.9 Ag contacts on rear side after metallization process 23

Figure 3.10 X-Ray Diffraction measurement device 24

Figure 3.11 SEM Measurement device 25

Figure 3.12 The UV-VIS-NIR device 26

Figure 3.13 I-V measurement device 27

Figure 3.14 Time-Resolved Photoresponse (I-t) measurement setup 28

Figure 4.1 XRD pattern of TiO2 deposited on glass substrate 29

Figure 4.2 Top-surface and cross-sectional SEM images of the TiO2 layer 30

Figure 4.3 Absorbance spectra of the deposited TiO2 layer. The inset of Fig. 4.3 shows Tauc plot for the layer 31

Figure 4.4 Current-voltage (I-V) curves of the photodiode 32

Figure 4.5 The transient response characteristics of the device 33

CHAPTER 1

INTRODUCTION

Metal oxide thin films such as TiO_2, ZnO, CuO_2, and SnO_2 have been important research subject for many technologies such as diodes, solar cells, and optical devices [1-8]. The improvement of these metal oxide thin films via low-cost fabrication has caused to comprehension of different electronic and optoelectronic devices [9-12]. Among the other metal oxide structures, TiO_2 is one of the important materials because of its chemical stability, relatively hard, cheap, and transparent properties. Also, TiO_2 is a wide band gap semiconductor providing photoconversion properties in the UV spectrum range.

TiO_2 has been extensively investigated in the fields of energy conversion and environmental protection [13]. During the past two decades, TiO_2 has shown a great potential as a promising photocatalyst in the treatment of water pollutants [14]. TiO_2 is limited due to the recombination rate of electron-hole pairs. In consequence, to make TiO_2 photoactive material, it can be doped with metal and non-metal elements. This doping process can be so effective to imrove electrical and optical properties of metal-oxides such as electrical conductivitity and absorption [15-28]. For example, doping process of TiO_2 with metal elements is an effective on the photoresponse property of TiO_2.

In recent years, there is a tendency to thin film technology for researchers. For solar cell devices which silicon based or heterojunction structures, TiO_2 can be used for important functions such as an n-type semiconductor layer, Transparent Conductive Oxide (TCO) layer, or an Anti-Reflecting Coating (ARC) layer absorption [3-4] [29-30].

Different methods such as Electron Beam Evaporation, Magnetron Sputtering, Chemical Vapor Deposition, Sol-Gel Spin Coating etc have been used to prepare thin films [31-34]. The selection of fabrication methods for the film deposition is important to acquire good electrical and optical properties. Among these methods, two stage

hydrothermal deposition method is commonly preferred for many researchers because of low cost, easily production and process controlling. Two stage hydrothermal method include nucleation and crystal growth processes [35].

Properties of thin films can be changed with using different experimental procedures. At this point, reaction temperature, reaction time or substrate type are important parameters for thin film properties. Modification of this parameters is so effective on thin film layer which be used for different applications. On the other hand, thin film modifications can significantly affect the structure performance for photovoltaic applications absorption [3-4] [29-30] [36].

For example, reaction temperature which annealing is effective factor on electrical characteristics of thin film. Consequently, changing of one parameter can be effective case on other characteristics.

Associated with material size becomes smaller and nanometer scale, new chemical and physical properties show up. These properties also change according to the shapes of nanomaterials such as nanorods, nanowires, nanosheets or nanotubes. For this reason, there are a lot of reviews and reports for the excellent nanomaterials which prepared via different methods. To produce nanomaterials there are many different methods such as sol-gel method, hydrothermal or solvothermal method, direct oxidation method, chemical vapor deposition, physical vapor deposition, and electrodeposition. Among these methods, to synthesize nanomaterials the hydrothermal method is commonly used baceuse of grain size, particle morphology, surface properties, and crystalline phase can be controlled with processing variables like composition of solution, pH value, reaction temperature, reaction time and pressure.

TiO_2 is a most widewhere worked material for industrial applications from the point of efficiency value, chemical and physical stability, and cost. TiO_2 nanomaterials are important structures owing to their numerous and multifarious applications such as environmental and biomedical applications, photovoltaic applications, water purification, biosensing area and drug delivery. In 1938 a study was declared on the photobleaching of dyes by TiO_2 [37]. In 1956, the generation of H_2O_2 from the solvent oxidation underneath UV irradiation and environmental aspects was investigated after

dispersing TiO_2 powders [38]. However, the photocatalytic performance of TiO_2 was not considered until electrochemical photolysis of water was explored by Fujishima and Honda [39]. In 1977, Frank and Bard investigated the photocatalytic oxidation ability of TiO_2 for the decomposition of cyanide in TiO_2 suspensions [40]. The first synthesis of n-TiO_2-based nanotubes was reported by Hoyer in 1996 with electrochemical deposition method [41]. Afterwards, the generation of TiO_2 nanotubes produced with hydrothermal method was reported [42-43].

The morphological structure of TiO_2 has a significant effect for its photovoltaic activity. Nanorods, nanoflowers, nanowires or nanotubes are one-dimensional nanostructures of TiO_2, and they have been researched because of their charge separation ability. In addition, they submit a way for charge carrier transport. Especially, about the environmental such as photocatalysis and energy topics such as water splitting, photo-/electrochromics or solar cells, preparation, applications, and modifications of TiO_2 nanomaterials are one of the most frequently studied research topics. TiO_2 nanorods can promote light harvest by multiple reflections [44-46] and allow for convenient walk path for photogenerated carriers [47]. Then, separation of electron-hole pairs and charge transport capability can be enhanced by TiO_2 nanorods as well.

In recent years, metal oxide semiconductor-based *p-n* heterojunction devices have been demonstrated to be an alternative technology for homojunction devices because of their advantages such as easy and cost-effective processes [6-8]. The p-n heterojunction structures are most studied materials for different applications like photodetectors, solar cells, and photodiodes [48-50]. Photodiode and solar cell sturectures are classified according to current-voltage characteristics. If there is an opening in third quadrant of I-V curve this structure exhibits photodide behaviour. In addition, if there is an opening in fourth quadrant of I-V curve this structure exhibits solar cell behaviour.

In this work, chapter one presents introduction of TiO_2 based works. In chapter two, the fundemandal working princible of p-n junction devices is explained. In chapter three, experimental details covering deposition and characterization of TiO_2/Si photodiodes are given. In chapter four, experimental results and discussion are presented. Finally, conclusions and future remarks are highlighted.

CHAPTER 2

TiO_2 BASED P-N HETEROJUNCTION STRUCTURES

2.1 Material Properties of TiO_2

Recently, titanium dioxide (TiO_2) has received a remarkable attention for scientific researchers because of its wide range applications. Due to its abundance, durability, strong optical absorption, transparency to the light of visible region, non-toxicity, high chemical and themal stability, high dielectric constant and high refractive index [51-54], it is preferred such applications especially for photovoltaic and sensors [55]. These applications can be divided in environment and energy categories which depend on properties and modifications of TiO_2 material with another materials. For environmental concerns, TiO_2 is extensively used for photodegradation of organic and inorganic pollutants [56], photovoltaic energy production [57], and hydrogen production by water photo-splitting [58-60]. For energy concerns, TiO_2 is an important photoactive material for instance photocatalytic contaminants oxidation [61-64], water splitting [65-66] and solar cells [67-69].

In addition, TiO_2 is a direct band gap semiconductor, it permits optoelectronic applications, dark condition, and UV illumination. Associated with other properties, TiO_2 is useful for fabricating many devices in the manner photodiodes, thin film solar cells, sensors, transparent thin-film transistors (TFTs) and many others.

TiO_2 can be formed in three different phases as brookite, rutile and anatase. The anatase and brookite are metastable phases and rutile is the most stable phase. The undoped TiO_2 is widely considered to be a strongly n-type semiconductor because of oxygen vacancies in the TiO_2 lattice. Group III elements which Ga, In, B, and Al act as donor in TiO_2 enhancement its n-type semiconductor behavior. TiO_2 has large excition binding energy that 458,5 eV and ~3.2 eV band gap value at room temperature which ensured important performance in the ultraviolet region. On the other hand, TiO_2 has three different crystalline structures which rutile, anatase and brookite under

environmental aspects. The rutile phase has high refractive index, and anatase phase has higher electrical mobility than rutile structure.

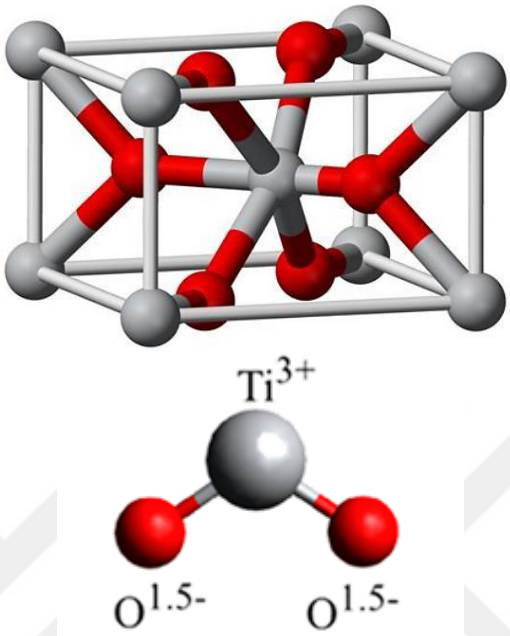


Figure 2.1 Schematic structure of TiO_2 [70]

Depending on using areas, TiO_2 thin films can be prepared using variety processes like Plasma Enhanced Chemical Vapor Deposition (PECVD), Radio-frequency Magnetron Sputtering, Metal-Organic Chemical Vapor Deposition, Spray Pyrolysis, Chemical Bath Deposition, Sputtering, Electrochemical Deposition, Sol-Gel Spin Coating, Photo-deposition, Atomic Layer Deposition and many others [71-74] opportunity of deposition on large area substrates, good microstructure, higher homogeneity and purity. Compared processes which using for preparation of TiO_2 thin film especially Chemical Bath Deposition method that connected with two stage hydrothermal deposition technique has been rather used for the nanocrystalline TiO_2 thin films preparation because of low temperature processing, low power consumption, least expensive, easily controllability and reliability.

Besides, Chemical Bath Deposition method can provide opportunity of depositing on substrates, good microstructure, higher homogeneity and purity. On the other hand, non-vacuum systems or methods are very attractive due to theire cost effective and

large using area. In Table 2. 1, some important parameters for rutile phase of TiO_2 are given.

Table 2.1 Properties of TiO_2

Parameter	Value
Density (g/cm^3)	4.23
Molar Mass (g/mol)	79.9378
Melting Point (°C)	1843
Band Gap Energy (eV)	3.23
Fermi Energy (E_F)	14.52
Refractive Index	2.54-2.72
Dielectric Constant	31
Light Absorption (nm)	<385
Resistivity (Ω cm)	$1.74x10^1$
Conductivity (Ω^{-1} cm^{-1})	$5.74x10^{-2}$
Sheet Resistance (Ωsq)	$1.94x10^6$
Sheet Carrier Mobility ($cm^2V^{-1}s^{-1}$)	4.15

2.2 TiO_2/p-Si Heterojunction Structures

There are a lot of studies on TiO_2/p-Si structure in the literature. In more recent years, TiO_2 based photodiode structures like the Schottky [75-76], metal-semiconductor-metal [77], n-TiO_2/p-TiO_2 homo junction [78] and TiO_2 thin film-based heterojunction photodiodes [79] [80-81] have been discovered for the UV applications. Jhaveri et al. [82] studied hole-blocking Si heterojunction using TiO_2 as the wide band gap material. Surface spectroscopy shows that the band-alignment at the Si/ TiO_2 interface is such that there is a large difference between the valence bands of Si and TiO_2 which prevents conduction of holes from Si and TiO_2.

The n-TiO_2/p-Si heterojunctions are perhaps the simplest Si-based UV photodiode which can be easily fabricated simply by depositing an n-TiO_2 layer on a p-Si substrate. Further, the heterojunction structures offer an easy fabrication method

combined with a low dark current [83] and effective way to improve the photocatalytic activity of TiO_2 [84]. n-TiO_2/p-Si structures are very much attractive for UV detection applications. In this view, Chang et al. [85] fabricated an ITO/n-TiO_2/Si diode structure using the atomic layer deposition (ALD) technique to study effects of the TiO_2/Si heterojunction and ITO-TiO_2 Schottky junction on the photo carrier transport direction in the device.

Sani et al. [86] fabricated n-TiO_2 nanowire/p-Si heterojunction diodes by the thermal evaporation method and studied the optoelectronic properties and measured a responsivity of 0.034 A/W at -4 V bias voltage. Recently, Selman et al [87] reported a sensitivity of ~$3.79x10^2$ at 5V bias for 325 nm incident UV light (1.6 mW/cm^2) for a n-TiO_2/p-Si heterojunction UV photodiodes fabricated by first growing a TiO_2 seed layer on the p-Si substrate by the RF sputtering method and the depositing an n-TiO_2 nanorods on the samples (with seed layer) by CBD method. One possible approach to low-cost silicon photovoltaics involves replacing the p-n junction, fabricated at temperatures higher than 800°C [88], with a low temperature fabricated heterojunction. Previously a solar cell using a silicon/P3HT heterojunction has been demonstrated with a power conversion efficiency of larger than 10%, as well as a solar cell using a silicon/PEDOT:PSS heterojunction with an efficiency of 12% [89-91].

Recently, because of various advantages of TiO_2/p-Si heterojunction that represented in Figure 2.2 structures many research groups study on this topic. This compound is preferred as an efficient material because of its easy fabrication process and low temperature experimental conditions. The bulk heterojunctions which obtained by TiO_2 thin films on p-Si substrates have been widely explored for ultraviolet (UV) detection [92] due to natural n-type wide bandgap semiconductor nature of TiO_2.

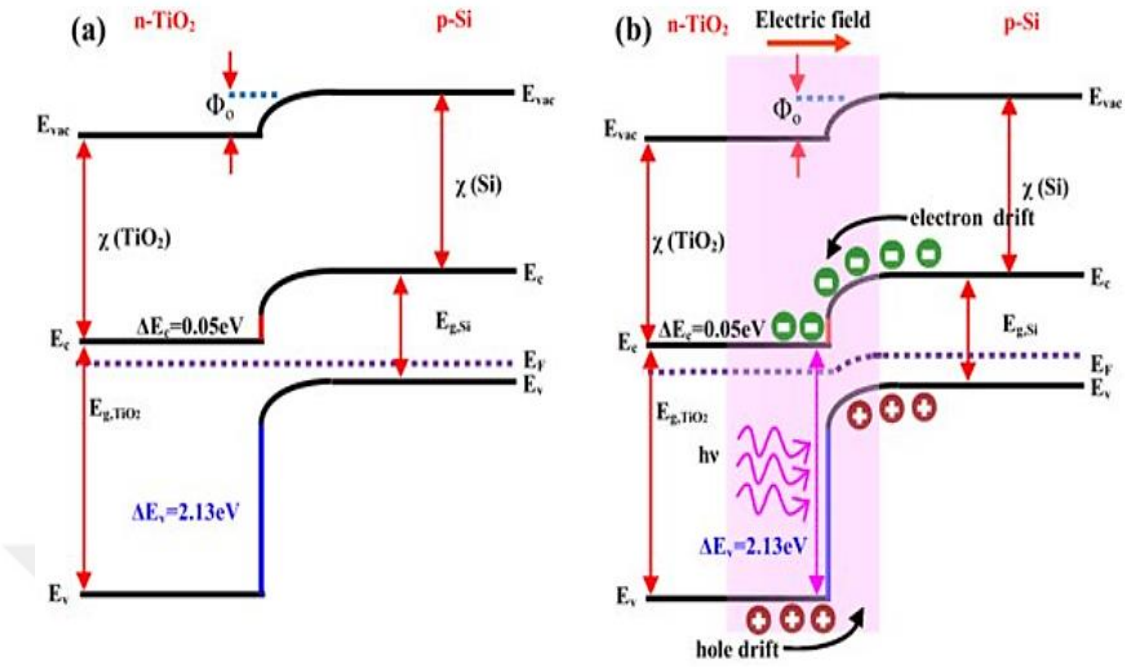


Figure 2.2 Energy band diagram of n-TiO_2/p-Si heterojunction (a) in the dark (b) under light [93]

The absorption ability of incident light and TiO_2 potential connected with energy band configuration of TiO_2. To exploit solar energy more effectually, it is necessity to find out and enhance longwave-light-sensitive TiO_2 photocatalysts with outstanding performance [94].

2.3 Working Principle of p-n junction-based Photodiodes

The behaviour of semiconductor devices that have heterojunction structure connected with energy bands alignments at the interfaces. These interface structures of heterojunctions are classified for three groups on the brink type I that referred as straddling gap, type II that referred as staggered gap and type III that referred as broken gap as shown in Figure 2.3.

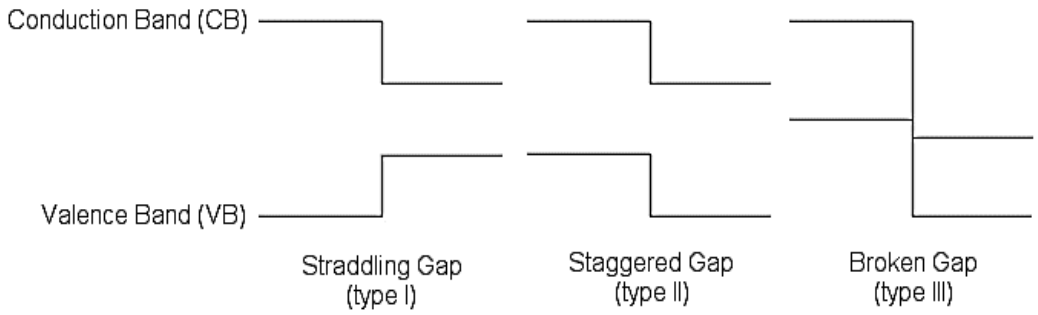


Figure 2.3 Different types of heterojunctions [95]

According to Figure 2.3, type I that referred as straddling gap the conduction band of second semiconductor device is lower than first semiconductor device, at the same time valence band of second semiconductor device is higher than first semiconductor device. Therewith the band gap of first semiconductor is higher than band gap of second semiconductor. For the type II that referred as staggered gap the conduction and valence band of second semiconductor device are lower than bands of first semiconductor device. In type II condition, the charge transformation is easier and more effective than other types which type I and type III. In type III that referred as broken gap conduction band of second semiconductor overlaps with the valence band of first semiconductor device. In view of this case, there is not forbidden energies in the interface, then the band gap of second semiconductor device is not bounded by band gap of first semiconductor device.

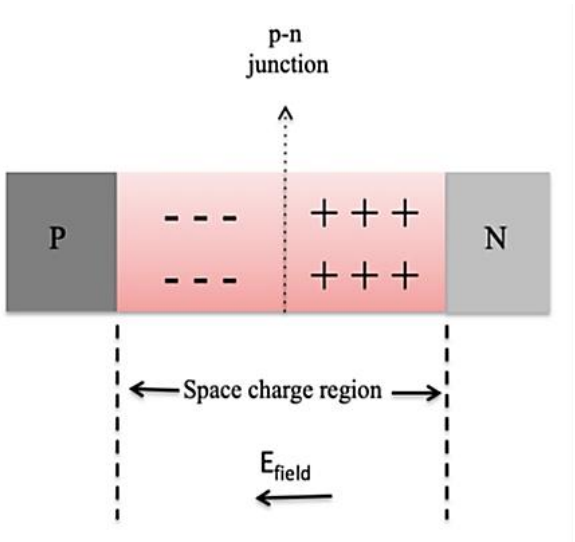


Figure 2.4 Structure of the p-n junction diode [96]

The working principles of a lot of electronic devices such as transistors, photodetectors, photodiodes, solar cells, LEDs and laser diodes are based on p-n junction structure. The p-n juntion structure is a boundary or an interface between p- and n- type regions in semiconductor materials. For p-type semiconductor materials, positive charges that holes are majority carriers and negative charges that electrons are minority carriers. In addition, for n-type semiconductor materials, positive charges that holes are minority carriers and negative charges that electrons are majority carriers. A p-n junction is formed by physical contact between p- and n-type materials. The band diagram of p-n juntion is demonstared in Figure 2.5.

Because of the change carrier concentration difference between p-type and n-type regions, diffusion occurs. At this point, diffusion of electrons from n-type to p type region and holes from p-type to n-type region occurs that results in positively and negatively charged region. The depletion region that called space-charge region at the same time is an area where charge transition occurs between p-type and n-type regions as illustrated before. Generally, it is called depletion region, due to it is effectively depleted of holes and electrons. Remaining region of each side of the semiconductor is called as quasi-neutral region [97].

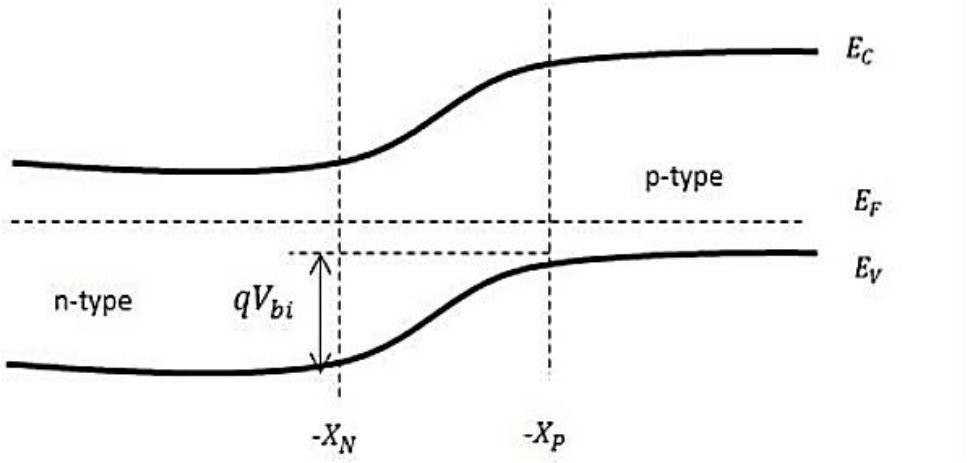


Figure 2.5 Band diagram of p-n junction [97]

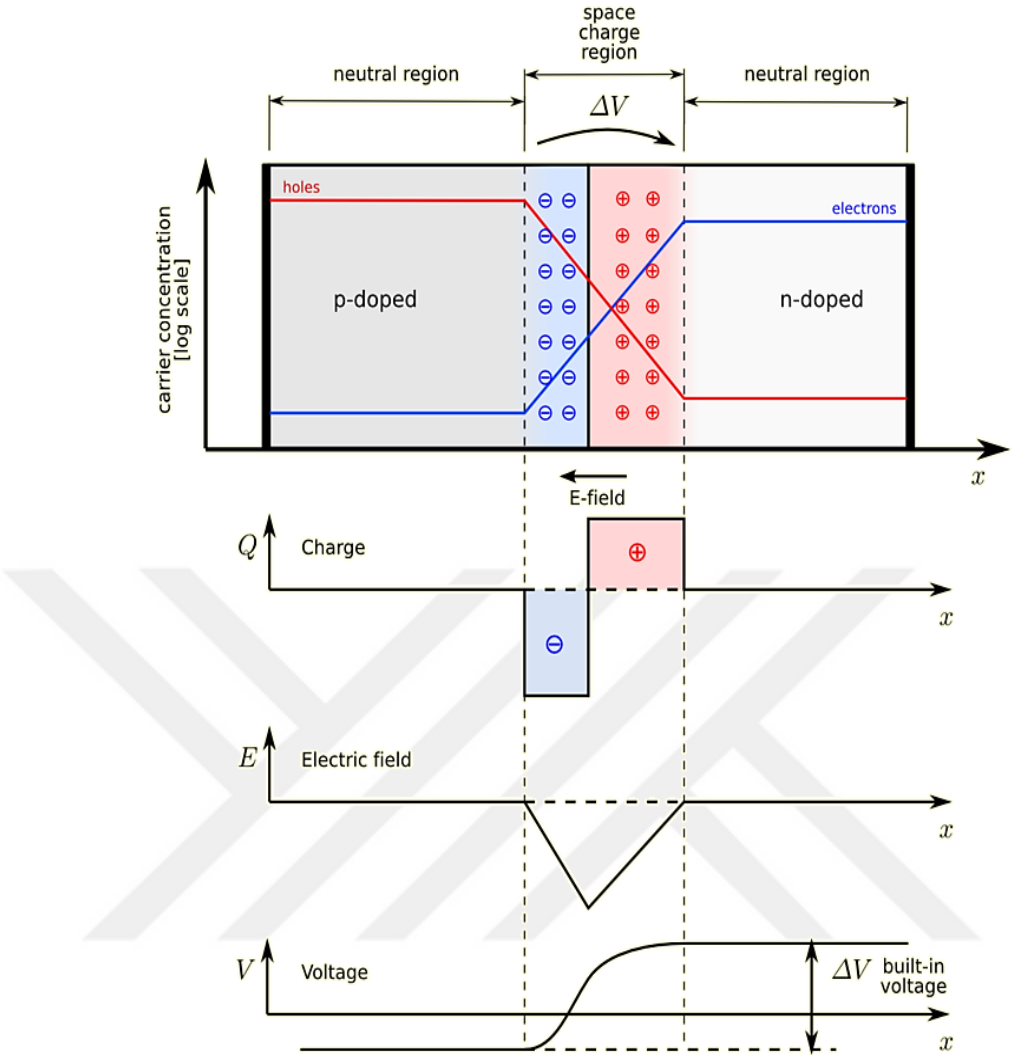


Figure 2.6 Band diagram of p-n junction diode under themal equilibrium [98]

If there is not any external input such as applied voltage in a p-n junction, this case is called a p-n juntion in thermal equilibrium conditions (zero bias) and illustrated in Figure 2.6. The currents balance each other out so there is not net current within device. In addition, the electric field (E_{field}) is generated by the space charge region opposes the diffusion process for electrons and holes. The direction of the internal electric field is from n- to p-type. Because of the change of energy level, the electric field that in p-n junction region causes a potential difference. An equilibrium condition in p-n junction occurs because of potential difference between p- and n-type regions. This potential difference is called built in potential (V_{bi}). The electric field between p-n

junction restrains more carriers from crossing junction and forms a barrier voltage (V_B) or V_{bi} in depletion region.

The meaning of forward bias condition in p-n junction diode; as illustrated in Figure 2.7, p-type semiconductor is connected to positive voltage terminal and n-type semiconductor is connected to negative voltage terminal. This case brings about the positive charges that holes in the p-type region and negative charges that electrons in the n-type region to be pushed toward the p-n junction. Then, depletion region is neutralized, and its width reduces. Besides, positive potential that applied to p-type region repels the holes, and negative potential that applied to n-type region repels the electrons. Through applied voltage, potential difference diminishes. At forward biases, the physical mechanism of forward capacitance is very comlex.

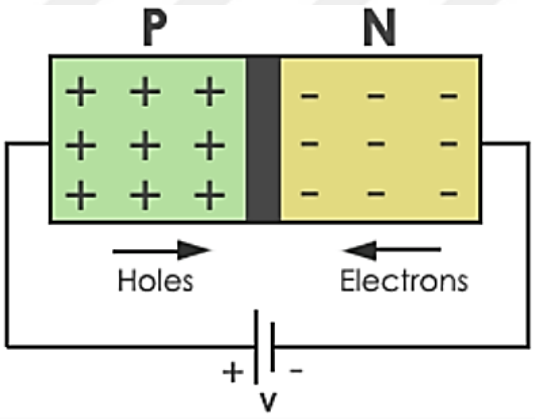


Figure 2.7 Band Diagram of p-n junction diode at forward bias [99]

In reverse bias, as an illustrated in Figure 2.8 p-type region is connected to the negative terminal of the battery, in addition n-type region is connected to the positive terminal. If diode is reverse biased, cathode voltage is higher than anode voltage. For this reason, a small current that nano amperes to micro amperes can flow until the diode breaks down. A voltage barrier raises that causing a high resistance to the flow of charge carriers which electrons and holes. In this way, minimum electrical current can pass through the p-n junction. Thereby, the increment of resistance in p-n junction bring about the junction behave like an insulator material. Photodiode devices are sensitive structures to light in third quadrant of I-V curve because of the characteristic behavior. For this reason, this study focused on concentrated reverse region behavior.

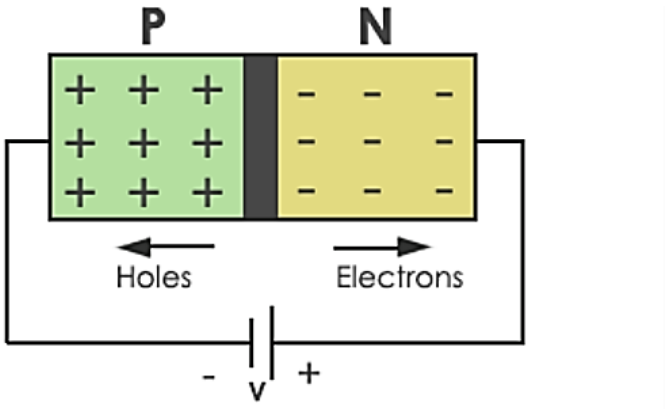


Figure 2.8 Band Diagram of p-n junction diode at reverse bias [99]

2.4 Evaluation of Photodiode Parameters

Photodiodes are semiconductor devices that sensitive for high energy particles and photons. In addition, photodiodes work by absorbing photons that come from light source or charged particles. A photodiode also creates a current flow in the circuit proportionaly with the power. A photodiode converts light to electrical current. When photons are absorbed by a photodiode, the current is generated. The photodideos reflected by an equivalent circuit are similar to solar cells. According to Figure 2.9, light current density is represented by J_L, dark current density J_D, series resistance R_s, shunt resistance R_{sh}, junction capacitance C_j in the circuit.

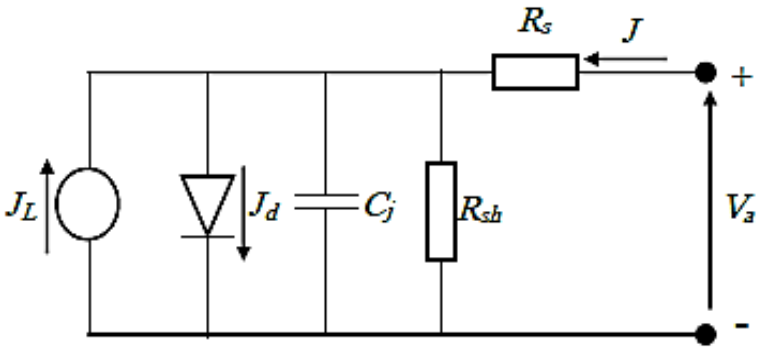


Figure 2.9 The equivalent circuit of photodiode [100]

In Figure 2.10 shows the reverse bias characteristics current density- voltage (*J-V*) curves of photodiode devices for dark and light conditions. As it is seen in this figure, sensitivity of a photodiode to light determined with reverse voltage value. Because the ratio value of J_D to J_L is reverse voltage dependent.

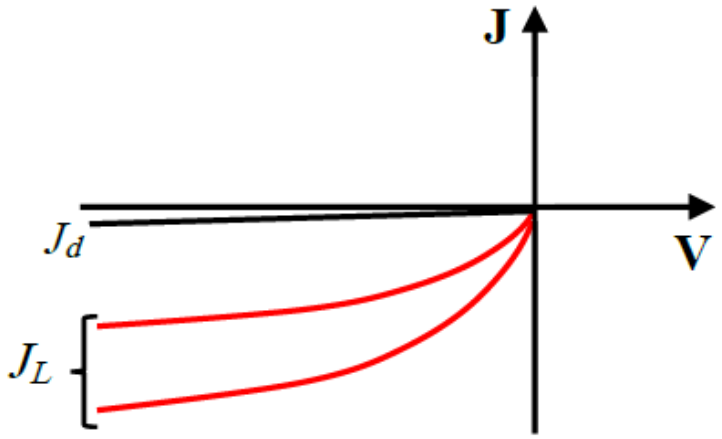


Figure 2.10 The reverse bias characteristics of photodiode devices under dark and light conditions [101]

A photodiode is represented by a current source in parallel with a diode as referred in Figure 2.10 and the current generated under favour of incident radiation. The determination of photodiode performance relates to reverse bias characteristics under dark and light conditions in *J-V* curve. The performance of a photodiode is evaluated as far as light sensitivity, the rise/fall time and frequency response.

Two important photodiode parameters which photosensitivity and photoresponsivity are determined with light sensitivity.

- The photoresponsivity, *PR (λ)* (A/W) of a photodiode is a value of the ratio of sensitivity to light, and it is described as of the ratio photocurrent J_L to incident light power P_{in}, where:

$$PR = \frac{J_L}{P_{in}} \quad \textbf{(2.1)}$$

To put it another way, the photoresponsivity is a measurement of the effectiveness of light power conversion in electrical current. It changes according to wavelength of incident light.

- The photosensitivity, *PS* is a value of the light current density J_L to dark current density J_D, where:

$$PS = \frac{J_L}{J_D} \quad \textbf{(2.2)}$$

- The rise time and fail time of a photodiode is identified like the time for signal to rise or fall from 10% to 90% or 90% to 10% of final value. The rise and fail times are stated as frequency response that is photodiode output decreases by 3dB.

$$t_r \cong \frac{0.35}{f_{3dB}} \quad \textbf{(2.3)}$$

- The specific detectivity, D^* [102] and Linear Dynamic Range, *LDR* [103] are important parameters for photodiodes to reflect signal detection ability. Linear dynamic is described a light intensity range is the current response of photodiode.

$$D^* = \frac{R\,A^{1/2}}{(2qI_{dark})^{1/2}} \quad \textbf{(2.4)}$$

$$LDR = 20\log(\frac{I_{Light}}{I_{dark}}) \quad \textbf{(2.5)}$$

- External Quantum Efficiency, *EQE* [104] is defined as the fraction of incident photons that contribute to current. In formula, h is Planck conctant, c is speed of light, q is electron charge and R is responsivity in nm.

$$EQE = \frac{hc}{q\lambda} Rx10^2\% \quad \textbf{(2.6)}$$

- Noise Equivalent Power, *NEP* is the amount of incident light power on photodiode that constituted a current equal to noise current. In formula, R_λ is responsivity and I_{tn} is total noise of photodiode.

$$NEP = \frac{I_{tn}}{R_\lambda} \quad \textbf{(2.7)}$$

CHAPTER 3

DEVICE FABRICATION

The fundamental structure for n-TiO_2/p-Si heterojunction photodiode is illustrated in Figure 3.1. The p-type Si substrate act as an absorber layer. In addition, TiO_2 layer is emitter layer that has high transparency. Silver (Ag) paste is used as of metal contacts for bottom and top contacts. TiO_2 metal oxide layer and TiO_2 nanorods (NRs) are sythenesized via two stage hydrothermal deposition method.

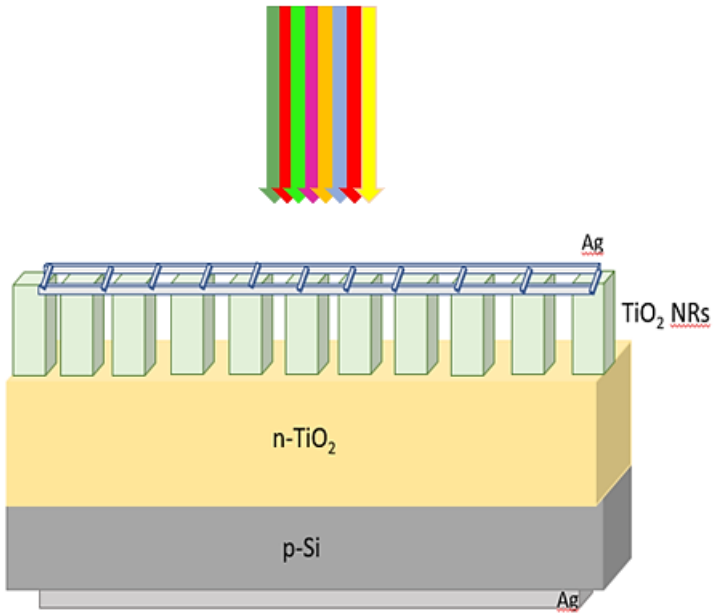


Figure 3.1 The fundamental structure of the photodiode

3.1 The Solution Preparation for TiO_2 Thin Film

In this section, the preparing of solutions which include two stage hydrothermal deposition method is explained. First stage is that to genereate n-TiO_2 thin film on glass and p-Si wafers. To prepare solution recipe for first stage, as a solvent de-ionized water (DIW) and as a precursor source of Titanium IV Chloride ($TiCl_4$) were used.

To second step of two stage hydrothermal deposition method relates to nanorod synthesize on p-Si substrates. In this study, glass samples were used just to

determination of absorbance and tranmittance of TiO_2 samples. For this reason, the second part of two stage hydrothermal deposition method were applied to p-Si wafers. The used chemical materials that used for second part of hydrothermal deposition method is given in Table 3.1.

Table 3.1 The materials and quantities for second part of hydrothermal method

Materials	Quantity (ml)
Titanium-IV Isopropoxide (TTIP)	0.8
Hydrochloric acid (HCI)	8
Acetic acid (HoAc)	16
Deiyonize water (DIW)	16

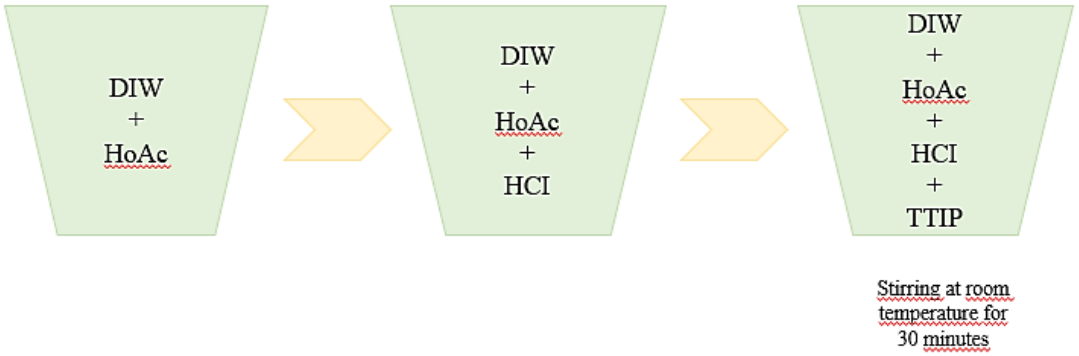


Figure 3.2 Preparation of the solution for second part of hydrothermal deposition

3.2 Cleaning Processes for Glass and p-Si substrates

The cleaning process differs between glass and p-Si substrates. Before cleaning process, all samples were cut for 1.5 cm x 1.5 cm sizes. Firstly, glass samples were kept in 10 ml aceton, 10 ml ethanol (EtOH) and 10 ml DIW for 10 minutes in ultrasonic bath device. Then, samples were dried with an air pump. To clean p-Si samples, two different solutions were prepared.

The first cleaning solution is called piranha solution that contains 30 ml Sulfuric Acid (H_2SO_4) and 10 ml Hydrogen Peroxide (H_2O_2). The second cleaning solution is called HF solution that contains 2 ml of Hydrofluoric Acid (HF) ve 38 ml of DIW.

Under favour of piranha solution organic and inorganic compounds can be eliminated from samples. Together with HF solution the surfaces of samples can be cleaned.

As shown in Figure 3.3, the p-Si substrates were immersed in the piranha solution at 80°C for 15 minutes with the using of stainless-steel tweezers to prevent corrosion in acid. Then, the bubbles were observed in the beaker during this time indicate that the samples have been cleaned. After, samples were kept in DIW for 1 minute to rinse process. After piranha solution, samples are dipped into the second cleaning solution that HF with Teflon tweezers to be kept at room temperature for 1 minute. Later, samples were kept in DIW for 1 minute at room temperature to rinse process. Once for all, for drying step samples were kept on the surface of magnetic stirrer and heated to 100°C for 10 minutes.

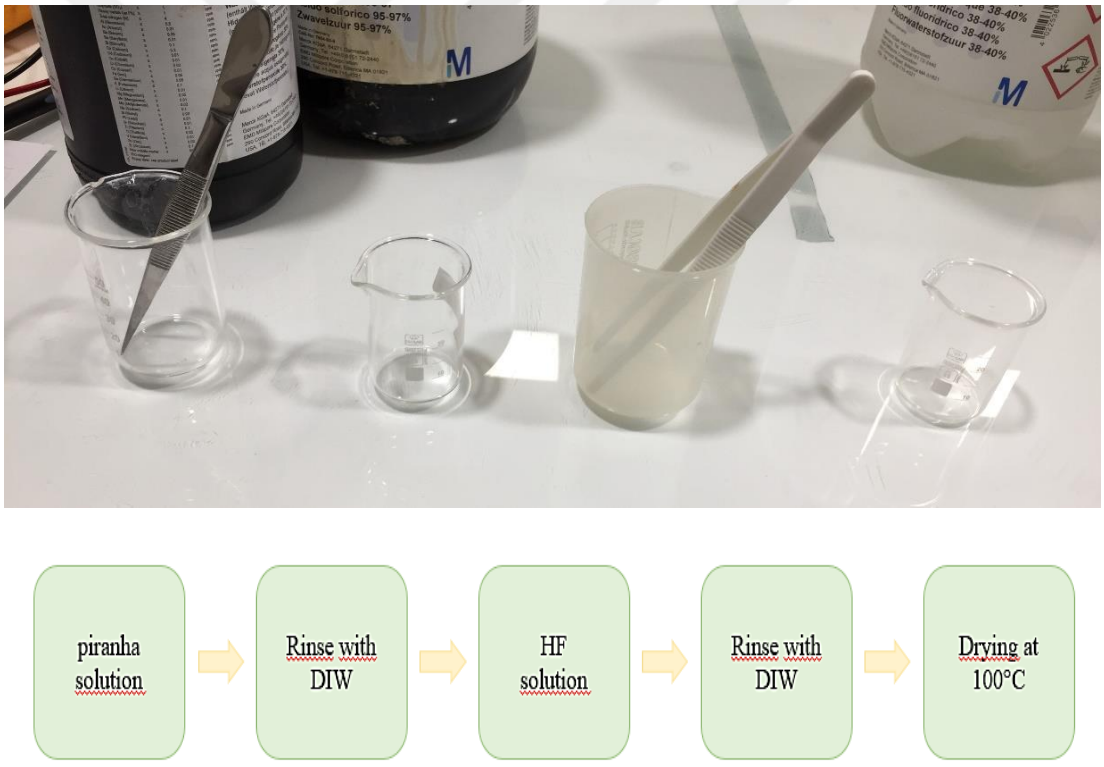


Figure 3.3 The cleaning process for p-Si substrates

3.3 Deposition

Before deposition process, to generate non-conductive SiO_2 thin film layer that has approximately 100 nm thickness on cutted and cleaned substrates which glasses and p-Si wafers, the heat treatment process was made in furnace at 800°C for 1 hour. Subsequently, to surface treatment for glass and p-Si substrates UV/ozone treatment process was applied to samples for 20 minutes as an illustrated in Figure 3.4.



Figure 3.4 UV/Ozone cabin

The deposition process includes two stage hydrothermal deposition method. Recipe information of first stage of deposition is that 2 ml of Titanium IV Chloride and 98 ml of deiyonize water were stirred to prepare solution. Then, as shows in Figure 3.5 the cleaned substrates which glasses and p-Si samples were put in solution and waited on surface of magnetic stirrer at 75°C for 40 minutes. After this step, samples were rinsed with pure water. Samples were kept on the surface of magnetic stirrer that heated to 50°C for 10 minutes for drying step. Once for all, samples were put in furnace at 450°C for 30 minutes for annealing that heat treatment process.

On the other hand, the second stage of deposition is about synthesize nanorods on p-Si wafers. According to Table 3.1 and Figure 3.2 the solution was prepared. The solution was stirred on surface of magnetic stirrer at room temperature for 30 minutes. After stirring step, as illustrated in Figure 3.6 the p-Si wafer samples were put in

Teflon-lined stainless-steel autoclave apparatus with solution and hydrothermal preparation was conducted at 150°C for 5 hours in furnace.

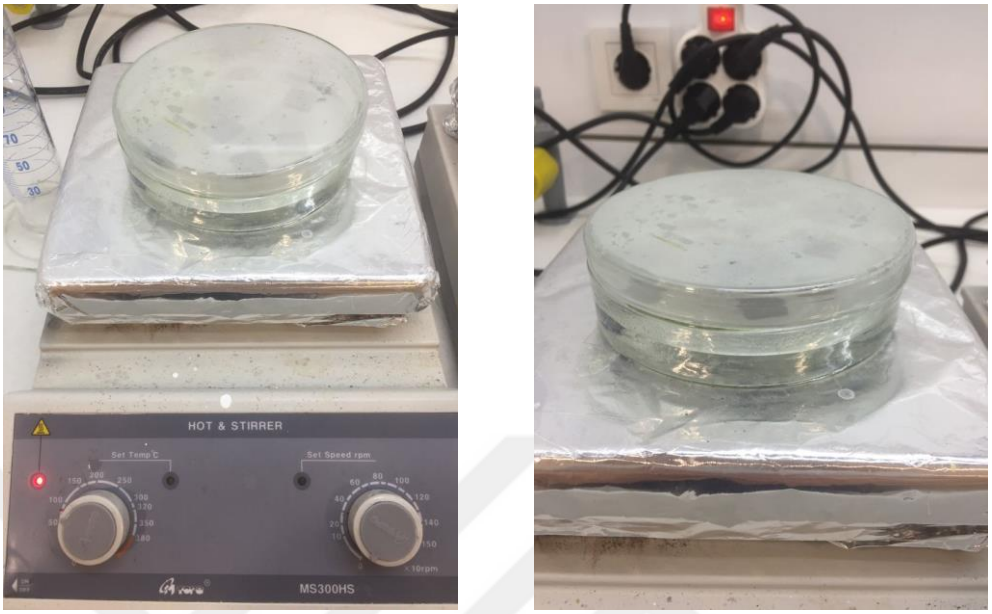


Figure 3.5 Glass and p-Si substrates located in solution

After hydrothermal deposition, the samples were rinsed twice. In conclusion, for drying step samples were kept on the surface of magnetic stirrer and heated to 100°C for 10 minutes.



Figure 3.6 p-Si wafers in autoclave apparatus

3.4 Metallization

Metallization process was applied to electrical current transfer in structure. At the same time, metallization process is realized by screen printing process. This process is applied to both front side and rear side of structure as illustrated in Figure 3.7. As it is understood from name, the metal deposition is made on the silicon substrates for screen printing process. The silver (Ag) paste was used to generate metal contacts for front side and rear side of structure. For applying Ag paste on surfaces, appropriate masks which different for front and rear side were used is illustrated in Figure 3.8 and Figure 3.9.

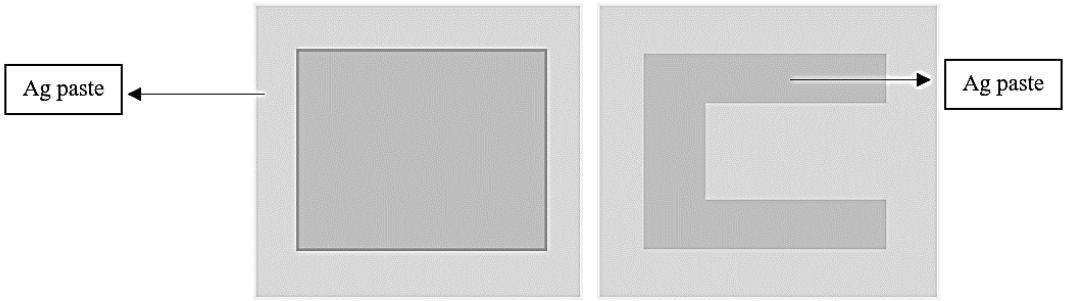


Figure 3.7 Screen printing masks for rear side and front side respectively

Screen printing process was applied to rear side with appropriate mask firstly. Then, samples were put into the tube furnace to dry at 150°C for 30 minutes. After removing the samples from tube furnace, the samples were allowed to cool down. Thereafter, the screen printing was applied to front side with an appropriate mask. And then, samples were put into the tube furnace to dry at 150°C for 30 minutes again.



Figure 3.8 Ag contacts on front side after metallization process

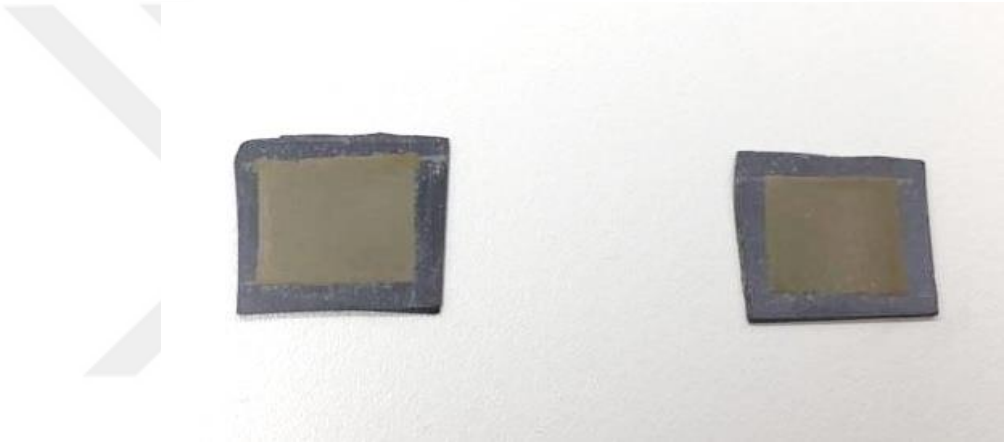


Figure 3.9 Ag contacts on rear side after metallization process

3.5 Characterizations

In this study, the experimental studies were made at Energy Systems Engineering Department Laboratory in Ankara Yıldırım Beyazıt University. The characterization processes were applied to specify of electrical, optical, and structural characterizastions of n-TiO_2/p-Si heterojunction photodiode device. In this context, X-Ray Diffraction (XRD), Scanning Electron Microscopy (SEM), UV-VIS-NR Spectrophotometer, Current-Voltage (I-V) and I-t measurements were made in laboratory.

3.5.1 X-Ray Diffraction (XRD) Measurement



Figure 3.10 X-Ray Diffraction measurement device

XRD is an analysis method that enables the determination of crystallographic properties of materials and the phases which they contain. In this study XRD measurement was made by Rigaku Miniflex,600 Table device as illustrated in Figure 3.10.

The working principle of XRD device is based on Bragg's law [105],

$$n\lambda = 2dsin\Theta \quad \textbf{(3.1)}$$

In this formula, n is the diffraction order, λ is the wavelength, d is grating constant, and Θ is measured from the surface normal. This XRD measurement was made between 20° and 60° with step size 0.02° using Cu-K_α radiations. Under favour of XRD measurement the thickness of thin films or multi-layers, atomic arrangement, structural

parameters such as lattice parameters, strain, grain size, phase composition of materials can be determined.

3.5.2 Scanning Electron Microscopy (SEM) measurement



Figure 3.11 SEM Measurement device

SEM is a type of electron microscope which obtains images by scanning methods the sample surface with a focused beam of electrons. Electrons interact with atoms in the sample to produce different signals which about topography and composition of the sample surface.

In addition, thickness and surface properties of materials can be determined via SEM measurement. In this study SEM measurement was made by Hıtachı SU5000 device which can work between 30x-1.500.000x range as illustrated in Figure 3.11.

3.5.3 UV-VIS-NIR Measurements



Figure 3.12 The UV-VIS-NIR device

The UV-VIS-NIR measurement device is used to determine light absorbance and transmittance of a material. In this study, this measurement is made with Shimadzu Corporation UV-1700 model device as illustrated Figure 3.12. This measurement is attenuation of a light beam after passes through a sample or is reflected from a surface. With this measurement, transparency value of material is measured with regards to percentage. Besides, absorbance value of material is measured in the sense of arbitrary unit (a.u).

3.5.4 Current-Voltage (I-V) Measurements

The facricated devices was measured to determine current-voltage (I-V) characteristics under dark and illumination conditions. The I-V measurement is implemented using four wire configuration that ensures more correct measurement than two wire configurations.

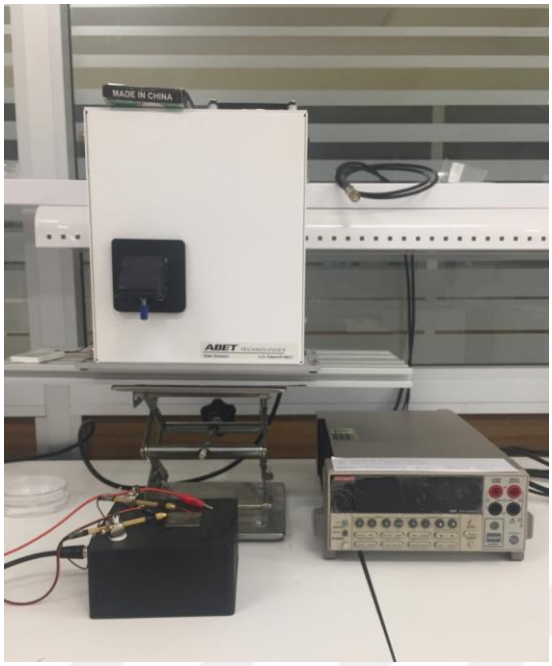


Figure 3.13 I-V measurement device

Current-voltage (I-V) measurement was used to appoint the electrical properties of n-TiO_2/p-Si device. The Figure 3.13 indicates the Keithley 2400 SMU source meter with a Abet LS 150 model solar simulator device which has AM1.5 irradiation that 1000 W/m^2. The I-V measurement device is connected to the computer. By this means, the measurement datas are captured to computer then I-V characteristics acquired.

3.5.5 The Time-Resolved Photoresponse (I-t) Measurements

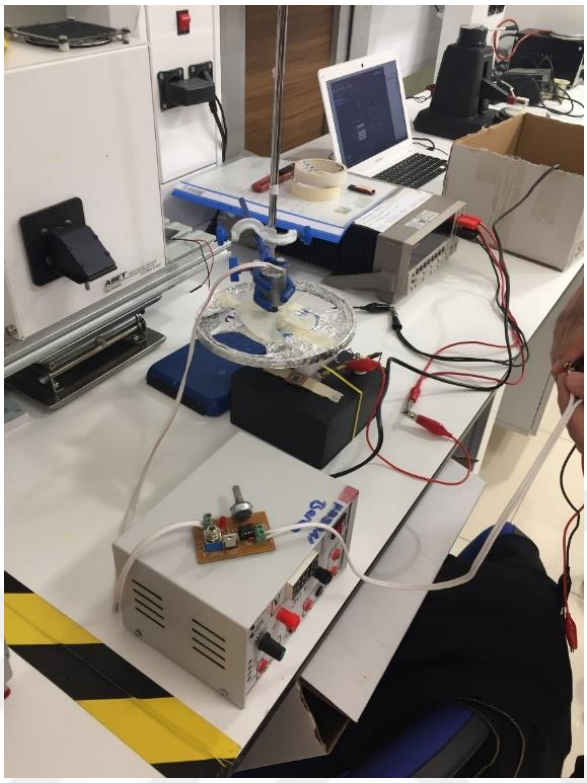


Figure 3.14 Time-Resolved Photoresponse (I-t) measurement setup

By courtesy of time-resolved photoresponse measurement, the electric current that passing through the photodiode is measured. The behavior of photodiode that under dark conditions and light illumination is determined with I-t measurement. In some ways, with this measurement it is concluded that how long the device takes to create an electron-hole pair.

CHAPTER 4

RESULTS AND DISCUSSION

4.1 X-Ray Diffraction Results

Initially, X-Ray Diffraction (XRD) measurement was realized to verify the deposition of TiO_2 layer. Figure 4.1 indicates the XRD pattern of TiO_2 layer deposited on glass substrate. From Fig. 4.1, one can observe four diffraction peaks corresponding to the (101), (004), (200) and (211) crystal planes, corroborating polycrystalline nature of the deposited TiO_2 layer (JCPDS file 21-1272) [106].

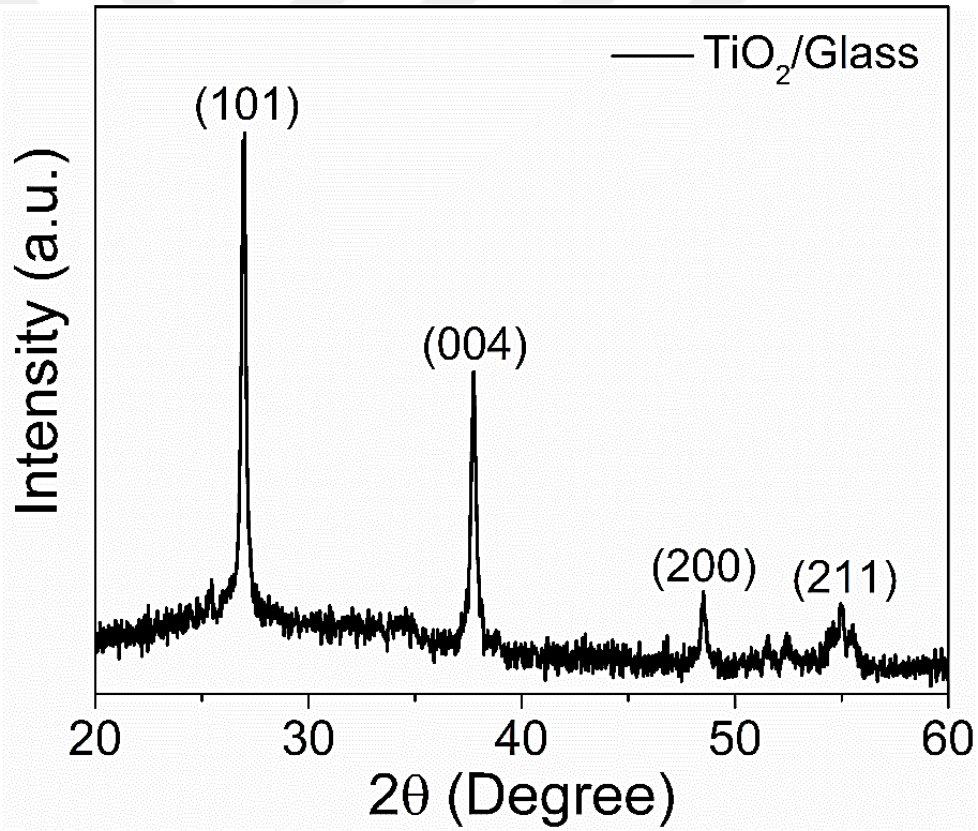


Figure 4.1 XRD pattern of TiO2 deposited on glass substrate

4.2 Scanning Electron Microscopy (SEM) Results

The morphology and the thickness of the TiO_2 layer were investigated by SEM. Figure 4.2 gives the top-surface and cross-sectional SEM images of the TiO_2 layer. As clearly observed from top-surface SEM image, TiO_2 layer was uniformly deposited on the Si substrates. In addition, one can easily express that TiO_2 nanorods (NRs) were homogenously grown via hydrothermal method. The thickness of the TiO_2 layer was determined by cross-sectional SEM image. As can be seen, it was found to be 2.81 μm (See the inset of Fig. 4.2).

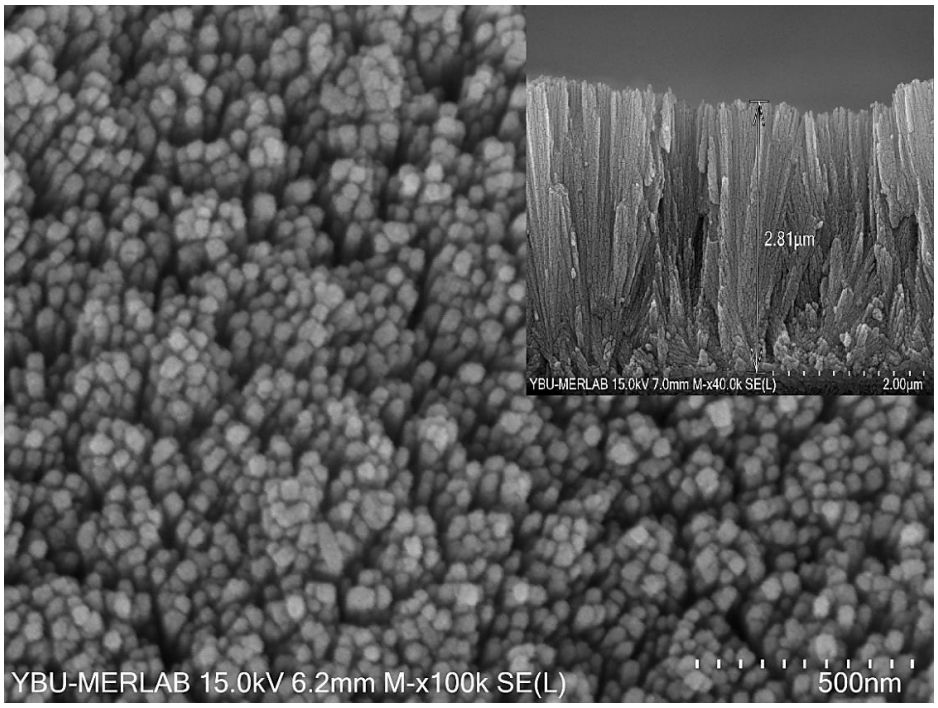


Figure 4.2 Top-surface and cross-sectional SEM images of the TiO2 layer

4.3 UV-VIS-NIR Results

The optical properties of the TiO_2 layer coated on the glass substrate is shown in Figure 4.3. Typically, it is worth mentioning that the obtained optical properties have the same optical behaviors as layers formed using metal oxides. As observed from Fig. 4.3, the sharp increase in absorption spectra indicates that the absorption edge of the TiO2 layer corresponds to about 365 nm. Herein, decreased absorbance in visible region implies that the deposited TiO_2 layer can be utilized as an emitter layer of p-n

heterojunction-based UV photodiodes. Employing Tauc equation, the bandgap size of the TiO_2 layer can be estimated:

$$(\alpha h\nu)^2 = c(h\nu - E_g) \quad \textbf{(4.1)}$$

Here α, hυ and C refer to the absorption coeffiecient, the incident photon energy and a constant. By extrapolating the plot of $(\alpha h\nu)^2$ versus hυ with a straight line, the value of Eg was evaluated to be 3.38 eV, which corresponds to a cut-off wavelength of 366 nm. Therefore, it makes sense to use a light source around and slightly above this cutoff wavelength to reveal the sensing capability of the device.

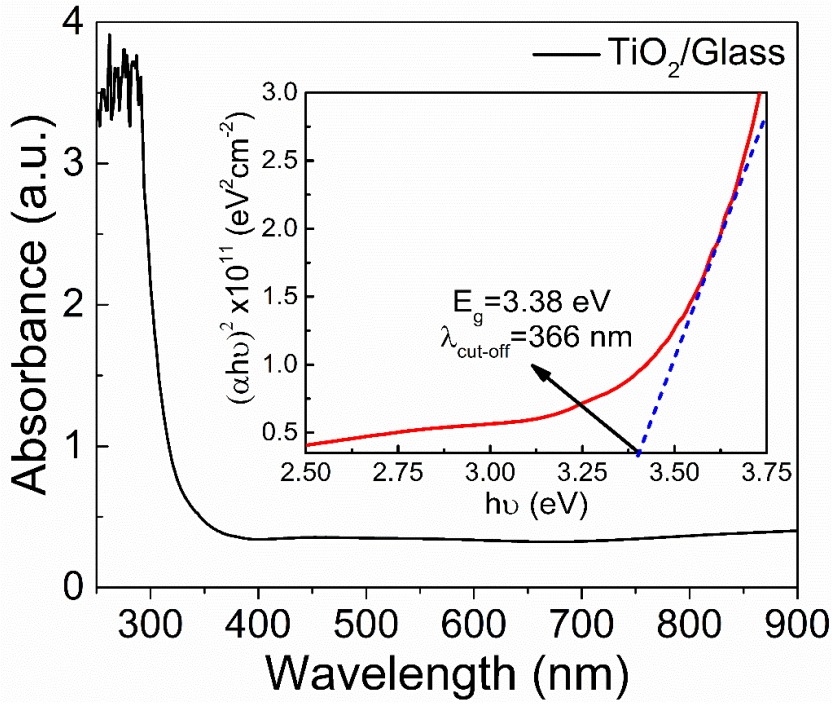


Figure 4.3 Absorbance spectra of the deposited TiO2 layer. The inset of Fig. 4.3 shows Tauc plot for the layer

4.4 The Current-Voltage Results

To assess the photoelectric performance of the device, the current-voltage (I-V) characteristics are measured in the dark and under irradiation. To quantitatively comprehend photodiode behavior, linear scale and semilogarithmic scale I-V characteristics of the device are shown in Figure 4.4. The linear I-V characteristics point out that the fabricated heterojunction exhibits a rectifying behaviour.

To evaluate the performance of the fabricated photodiode, some important performance parameters, that is to say responsivity (PR), sensitivity (PS), detectivity (D*), near equivalent power (NEP) etc., have to be calculated. These parameters can be determined by using aforementioned formulas. Ultimately, our device shows a responsivity (PR) of 1.41 A/W, sensitivity (PS) of 80, detectivity (D*) of 8.3×10^{11} Jones and near equivalent power (NEP) of 1.2×10^{-12}.

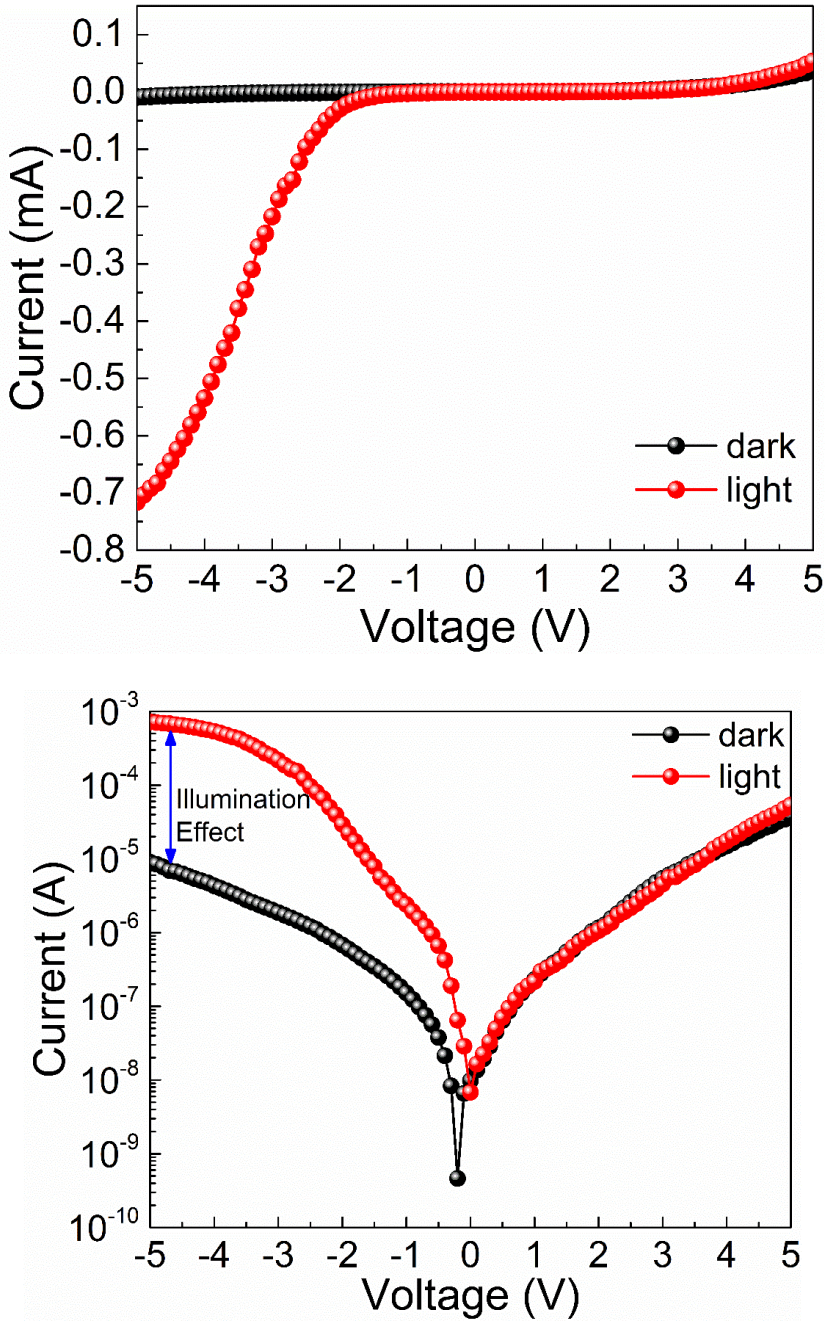


Figure 4.4 (a) Linear and (b) semilogarithmic-scale current-voltage (I-V) curves of the photodiode measured in the dark and under 365 nm UV irradiation

As seen from Fig. 4.4 (a), once the device is irradiated by 365 nm light, the light is absorbed by the sample, resulting in the generation of electron-hole pairs.

From Fig. 4.4 (b), one can observe that these photogenerated electron-hole pair, i.e. minority carriers, play a key role in determining photocurrent value of the device under reverse biased condition.

4.5 The Time-Resolved Photoresponse (I-t) Results

Rise time and decay time are key parameters that characterize the response speed of any photodetection based device. Figure 4.5 shows the transient response characteristics of the device measured under excitation of a 365 nm pulsed UV light source. From this measurement, the values of rise time (τ_r) and decay time (τ_d) were calculated to be 25 ms and 23 ms at -5V for TiO_2/p-Si heterojunction-based photodiode, respectively.

The obtained values of τ_r and τ_d show that the device has a fast photoresponse characteristics. This fast response property is directly correlated to the charge carrier separation and transportation property.

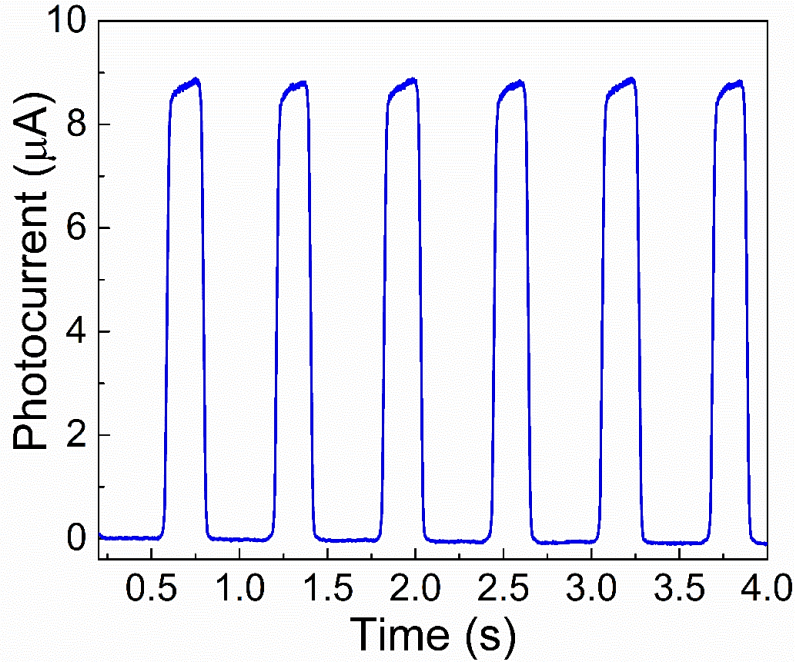


Figure 4.5 The transient response characteristics of the device measured under excitation of a 365 nm pulsed UV light source

Ultimately, our results point out that the fabricated sample exhibits a high UV sensing performance than its analogous. Table 4.1 displays the comparison of performance parameters of reported metal-oxide based UV photodiodes.

Table 4.1 Comparison of key parameters of reported metal-oxide based UV photodiodes

Device Structure	***PR*** **(A/W)**	***PS***	D^* **(Jones)**	τ_r/τ_d **(ms)**	**Ref.**
TiO_2 NRs/*p*-Si	1.41	80	8.32×10^{11}	25/23	This work
***n*-SnO_2/*p*-Si**	0.17	15	3.50×10^{10}	-	[107]
***n*-SnO_2/SiNW**	0.35	64	8.03×10^{12}	-	[107]
SnO_2/SiO_2/*p*-Si	0.35	180	2.66×10^{12}	<100	[108]
***n*-TiO_2/*p*-SiNW**	0.80	2.4	2.44×10^{8}	-	[109]
***n*-TiO_2/*p*-SiNW**	0.23	113	8.66×10^{11}	-	[110]
***n*-TiO_2/*p*-Si**	6.74	39	1.31×10^{12}	128/120	[111]
***n*-ZnO/*p*-Si**	0.35	19	4.16×10^{9}	-	[112]
***n*-TiO_2/*p*-Si**	1.25	4.2	1.62×10^{11}	-	[113]

CHAPTER 5

CONCLUSIONS

In this study, we assembled n-TiO_2 nanorods deposited on p-Si substrates via hydrothermal method to form a n-TiO_2/p-Si *p-n* heterojunction photodiode where photo-generated electrons travel from p-Si to n-TiO_2 over a barrier under illumination. The crystal structure, band gap energy and some important electrical parameters of the fabricated device have been excracted via X-Ray Diffraction, Scanning Electron Microscopy, UV-Vis Spectroscopy and Current-Voltage measurements. The results showed that the device is sensitive to ultraviolet light (365 nm). The fabricated photodiode showed excellent photosensitivity with a maximum photo responsivity of 1.41A/W, photosensitivity of 80, detectivity of $8.32x10^{11}$ Jones and a photoresponse time of 25 ms at 365 nm ultraviolet light.

For further study on n-TiO_2/p-Si *p-n* heterojunction photodiodes, the following suggestions can be considered to boost photodetection performance of the devices.

- ✓ The aspect ratio of TiO_2 nanorods can be tailored.
- ✓ The porosity ooccuring among TiO_2 nanorods can be managed.
- ✓ Some dopants can be introduced.
- ✓ Plasmonic nanoparticles can be added to the device structure.

REFERENCES

[1] Mardare, D., et al. Electrical conduction mechanism and gas sensing properties of Pd-doped TiO2 films. Journal of Non-Crystalline Solids, 357.7:1774-1779. 2011

[2] Serin, T., et al. Extraction of important electrical parameters of CuO. Physica B: Condensed Matter, 406.3:575-578. 2011

[3] Yildiz, A., et al. Enhancement of efficiency of natural and organic dye sensitized solar cells using thin film TiO2 photoanodes fabricated by spin-coating. Journal of Photochemistry and Photobiology A: Chemistry, 368:23-29. 2019

[4] Atli, A., Atilgan, A., & Yildiz, A. Multi-layered TiO2 photoanodes from different precursors of nanocrystals for dye-sensitized solar cells. Solar Energy, 173:752-758. 2018

[5] Serin, T., et al. Multiphonon hopping of carriers in CuO thin films. Physica B: Condensed Matter, 406.19:3551-3555. 2011

[6] Ozel, K., et al. A route towards enhanced UV photo-response characteristics of SnO2/p-Si based heterostructures by hydrothermally grown nanorods. Journal of Alloys and Compounds, 849:156628. 2020

[7] Sbeta, M., & Yildiz, A. Optical response enhancement of GZO/p-Si heterostructures via metal nanoparticles. Materials Research Express, 6.8:085018. 2019

[8] Ozel, K., & Yildiz, A. SnO2/ZnO/p-Si and SnO2/TiO2/p-Si heterojunction UV photodiodes prepared using a hydrothermal method. Sensors and Actuators A: Physical, 315:112351. 2020

[9] Sbeta, M., & Yildiz, A. Optical response enhancement of GZO/*p*-Si heterostructures via metal nanoparticles. Materials Research Express, 085018. 2019

[10] Ozel, K., & Yildiz, A. SnO2/ZnO/*p*-Si and SnO2/TiO2/*p*-Si heterojunction UV photodiodes prepared using a hydrothermal method. Sensors and Actuators A: Physics, 315 112351. 2020

[11] Yildiz, Z. K., Atilgan, A., Atli, A., Ozel, K., Altinkaya, C., & Yildiz, A. Enhancement of efficiency of natural and organic dye sensitized solar cells using thin film TiO2 photoanodes fabricated by spin-coating. Journal of Photochemistry and Photobiology A: Chemistry, 368 23–29. 2019

[12] Atli,A., Atilgan, A., & Yildiz, A. Multi-layered TiO2 photoanodes from different precursors of nanocrystals for dye-sensitized solar cells. Solar Energy, 173 752–758. 2018

[13] Fujishima, A., Rao, T. N., & Tryk, D. A. Journal of Photochemistry and Photobiology C: Photochemistry Review, 1–21. 2020

[14] Chong, M. N., Jin, B., Chow, C.W.K., & Saint, C. Recent developments in photocatalytic water treatment technology: a review. Epub, 44 2997– 3027. 2020

[15] Yildiz, A., Iacomi, F., & Mardare, D. Polaron transport in TiO2 thin films. Journal of Applied Physics, 108.8:083701. 2010

[16] Yildiz, A., et al. Influence of grain boundaries on the figure of merit of undoped and Al, In, Sn doped ZnO thin films for photovoltaic applications. Scripta Materials, 113:23-26. 2016

[17] Yildiz, A., et al. Ni doping effect on electrical conductivity of ZnO nanocrystalline thin films. Journal of Materials Science: Materials in Electronics 22.9:1473-1478. 2011

[18] Alsac, A. A., et al. Improved conductivity of Sb-doped SnO2 thin films. Journal of Applied Physics, 113.6:063701. 2013

[19] Yildiz, A., et al. Hopping conduction in In-doped CuO thin films. Applied Surface Science, 318:105-107. 2014

[20] Serin, N., et al. Estimation of compensation ratio by identifying the presence of different hopping conduction mechanisms in SnO2 thin films. Thin Solid Films, 519.7:2302-2307. 2011

[21] Horzum, S., et al. Monitoring the characteristic properties of Ga-doped ZnO by Raman spectroscopy and atomic scale calculations. Journal of Molecular Structure, 1180:505-511. 2019

[22] Yildiz, A., et al. Electrical conduction properties of Co-doped ZnO nanocrystalline thin films. Journal of Materials Science: Materials in Electronics, 23.2:425-430. 2012

[23] Yildiz, A., et al. Glancing angle deposited Al-doped ZnO nanostructures with different structural and optical properties. Thin solid films, 589:764-769. 2015

[24] Serin, T., et al. Electrical conduction properties of In-doped ZnO thin films. Physica Scripta, 84.6:065703. 2011

[25] Yildiz, A., Lisesivdin, S. B., Kasap, M., & Mardare, D. High temperature variable-range hopping conductivity in undoped TiO2 thin film, Optoelectronics and Advanced Materials-Rapid Communications, 1(10) 531-533. 2007

[26] Mardare, D., et al. Surface wettability of titania thin films with increasing Nb content. Journal of Applied Physics, 112.7:073502. 2012

[27] Yildiz, A., et al. The substrate temperature dependent electrical properties of titanium dioxide thin films. Journal of Materials Science: Materials in Electronics, 21.7:692-697. 2012

[28] Sbeta, M., et al. Influence of the spin acceleration time on the properties of ZnO: Ga thin films deposited by sol–gel method. Journal of Sol-Gel Science and Technology, 86.2:513-520. 2018

[29] Atli, A., et al. St. Lucie cherry, yellow jasmine, and madder berries as novel natural sensitizers for dye-sensitized solar cells. International Journal of Energy Research, 43.8:3914-3922. 2019

[30] Kocak, Y., et al. Extraction method dependent performance of bio-based dye-sensitized solar cells (DSSCs). Materials Research Express, 6.9 095512. 2019

[31] Bouabid, K., Ihlal, A., Amir, Y., Sdaq, A., Assabbane, A., Ait-Ichou, Y., Outzourhit, A., Ameziane, E. L., & Nouet, G. Optical study of TiO2 thin films prepared by sol-gel. Ferroelectrics, 372: 69-75. 2018

[32] Ha, H. Y., Nam, S. W., Lim, T. H., Oh, I. H., & Hong, S. A. Properties of the TiO2 membranes prepared by CVD of titanium tetraisopropoxide. Journal of Membrane Science, 111: 81-92. 1996

[33] Takeda, S., Suzuki, S., Odaka, H., & Hosono, H. Photocatalytic TiO2 thin film deposited onto glass by DC magnetron sputtering. Thin Solid Films, 392: 338-44. 2001

[34] Wang, S., Xia, G., He, H., Yi, K., & Shao, J. Structural and optical properties of nanostructured TiO2 thin films fabricated by glancing angle deposition. Alloys and Compounds 431:287-291. 2007

[35] Zhang, J., et al. A well-grown B-Ga3O3 microrod array formed fron GaOOH on a Si(100) substrate and growth mechanism study. Crystal Engineering Community, 20 4329–4335. 2018

[36] Yildiz, A., et al. Efficient Iron Phosphide Catalyst as a Counter Electrode in Dye-Sensitized Solar Cells. ACS Applied Energy Materials, 4.10:10618-10626. 2021

[37] Goodeve, C. F., & Kitchener, J. A. The mechanism of Photosensitisation by Solids. Journal of the Chemical Society,Faraday Transactions, 34 902–908. 1938

[38] Hashimoto, K., Irie, H., & Fujishima, A. TiO2 Photocatalysis: A Historical Overview and Future Prospects. Japanese Journal of Applied Physics, 44 8269–8285. 2005

[39] Fujishima, A., & Honda, K. Electrochemical Photolysis of Water at a Semiconductor Electrode. Nature, 238 37–38. 1972

[40] Frank, S. N., & Bard, A. J. Heterogeneous Photocatalytic Oxidation of Cyanide Ion in Aqueous Solutions at Titanium Dioxide Powder. Journal of American Chemical Society, 99 303–304. 1977

[41] Hoyer, P. Formation of a Titanium Dioxide Nanotube. Materials Sciences and Applications, 12 1411–1413. 1996

[42] Kasuga, T., Hiramatsu, M., Hoson, A., Sekino, T., & Niihara, K. Titanium Oxide Nanorods pH Sensors:Comparison Between Voltammetry and Extended Gate Field Effect Transistor Measurements. Materials Sciences and Applications, 14 3160 3163. 1998

[43] Zwilling, V., Darque-Ceretti, E., Boutry-Forveille, A., David, D., Perrin, M.Y., & Aucouturier, M. Structure and Physicochemistry of Anodic Oxide Films on Titanium and TA6V Alloy. Surface and Interface Analysis, 27 629–637. 1999

[44] Zhang, D., Wen, M., Zhang, S., Liu, P., Zhu, W., Li, G., & Li, H. Au Nanoparticles Enhanced Rutile TiO2 Nanorod Bundles with High Visible-light Photocatalytic Performance for NO Oxidation. Applied Catalysis B:Environmental, 147, 610-616. 2014

[45] Bian, J., Huang, C., Wang, L., Hung, T., Daoud, W. A., & Zhang, R. Carbon Dot Loading and TiO2 Nanorod Length Dependence of Photoelectrochemical Properties in Carbon Dot/TiO2 Nanorod Array Nanocomposites. ACS Appied Materials Interfaces, 6 4883-4890. 2014

[46] Zhou, Q., Zhang, S., Yang, X., Wu, Q., Zhao, H., & Wu, M. Rutile Nanowire Array Electrodes for Photoelectrochemical Determination of Organic Compounds Sensor Actuat. B, 186 132-139. 2013

[47] Mu, Q., Li, Y., Zhang, Q., & Wang, H. Template-Free Formation of Vertically Oriented TiO2 Nanorods with Uniform Distribution for Organics-Sensing Application. Journal of Hazardous Materials, 188, 363-368. 2011

[48] Ozel, K., & Yildiz, A. Comprehensive Understanding of the Role of Emitter Layer Thickness for Metal–Oxide–Semiconductors Based Solar Cells. IEEE Journal of Photovoltaics, 12.1 251-258. 2021

[49] Ozel, K., & Yildiz, A. Estimation of Maximum Photoresponsivity of n-SnO2/p-Si Heterojunction-Based UV Photodetectors. Physica Status Solidi (RRL)–Rapid Research Letters, 210049. 2021

[50] Ozel, K., & Yildiz, A The potential barrier-dependent carrier transport mechanism in n-SnO2/p-Si heterojunctions. Sensors and Actuators A: Physical, 332 113141. 2021

[51] Humayun, M., Raziq, F., Khan, A., & Luo, W. Modification strategies of TiO2 for potential applications in photocatalysis:a critical review. Green Chemistry Letters and Reviews, 86-102. 2018

[52] Xu, M., Da, P., Wu, H., Zhao, D., & Zheng, G. Controlled Sn-doping in TiO2 nanowire photoanodes with enhanced photoelectrochemical conversion. Nano Letters, 1503-1508. 2012

[53] Rossetti, I., Villa, A., Compagnoni, M., Prati, L., Ramis, G., Pirola, C., Bianchi, C. L., Wang, X., & Wang, D. CO2 photoconversion to fuels under high pressure: effect of TiO2 phase and of unconventional reaction conditions. Catalysis Science & Technology, 9 2253. 2015

[54] Aksoy, S., & Caglar, Y. Structural transformations of TiO2 films with deposition temperature and electrical properties of nanostructure n-TiO2/p-Si heterojunction diode. Journal Alloys and Compounds, 613-625. 2014

[55] Atli, A. et al. Optimizing Deposition Parameters of DSSCs Composed of Blue TiO2. IEEE Journal of Photovoltaics, 11.1:118-123. 2020

[56] Carp, O., Huisman, C. L., & Reller, A. Photoinduced reactivity of titanium dioxide. Progress in Solid State Chemistry, 32:33e177. 2004

[57] O'Regan, B., & Gratzel, M. Photoelectrochemical properties of Nb doped TiO2 semiconductor ceramic membrane. Nature, 353:737e9. 1991

[58] Fujishima, A., & Honda, K. Electrochemical photolysis of water at a semiconductor electrode. Nature, 238:37e8. 1972

[59] Dholam, R., Patel, N., & Adami, M. Physically and chemically synthesized TiO2 composite thin films for hydrogen production by photocatalytic water splitting. International Journal Hydrogen Energy, 33(23):6896e903. 2008

[60] Xu, S., Ng, J., Zhang, X., Bai, H., & Sun, D. D. Fabrication and comparison of highly efficient Cu incorporated TiO2 photocatalyst for hydrogen generation from water. International Journal Hydrogen Energy, 35:52e4. 2010

[61] Liu, Z., Zhang, X., Nishimoto, S., Murakami, T., & Fujishima, A. Efficient photocatalytic degradation of gaseous acetaldehyde by highly ordered TiO2 nanotube arrays. Environmental Science and Technology, 42, 8547. 2008

[62] Fujishima, A., Zhang, X., & Tryk, D. A. TiO2 photocatalysis and related surface phenomena. Surface Science Report, 63 515. 2008

[63] Chen, X., & Mao, S. S. Titanium dioxide nanomaterials: Synthesis, properties, modifications, and applications. Chemicals Reviews, 107 2891. 2007

[64] Chen, L., Graham, M. E., Li, G., & Gray, K. A. Fabricating highly active mixed TiO2 photocatalysts by reactive DC magnetron sputter deposition. Thin Solid Films, 515 1176. 2006

[65] Fujishima, A., & Honda, K. Electrochemical photolysis of water at a semiconductor electrode. Nature, 238 37. 1972

[66] Fujishima, A., & Honda, K. Studies on photosensitive electrode reactions. Bulletin of the Chemical Society Japan, 44 1148. 1971

[67] O'Regan, B., & Gratzel, M. A low cost, high-efficiency solar-cell based on dye-sensitized colloidal TiO2 films. Nature, 353 737. 1991

[68] Mor, G.K., Shankar, K., Paulose, M., Varghese, O.K., & Grimes, C. A. Use of highly ordered TiO2 nanotube arrays in dyesensitized solar cells. Nano Letters, 6 215. 2006

[69] Kongkanand, A., Tvrdy, K., Takechi, K., Kuno, M. K., & Kamat P. V. Quantum dot solar cells. Tuning photoresponse through size and shape control of CdSe-TiO2 architecture. Jornal of the American Chemical Society, 130 4007. 2008

[70] Daniel, K., & Sergei, M. On the Charge State of Titanium in Titanium Dioxide. The Journal of Physical Chemistry Letters, 1593–1598. 2017

[71] Martinet, C., Paillard, V., Gagnaire, A., & Joseph, J. Deposition of SiO2 and TiO2 thin films by plasma enhanced chemical vapor deposition for antireflection coating. Journal of Non-Crystalline Solids, 216:77e82. 1997

[72] Mulla, I. S., Soni, H. S., Rao, V. J., & Sinha, A. P. B. Deposition of improved optically selective conductive tin oxide films by spray pyrolysis. Journal of Materials Science, 21:1280e8. 1986

[73] Suzuki, S., Ohsaki, H., & Ando, E. Materialistic difference in macroscopic friction coefficients of sputtered metal oxide thin films deposited on glass. Japanese Journal of Applied Physics, 35:1862e7. 1996

[74] Bouabid, K., Ihlal, A., Amira, Y., Sdaq, A., Assabane, A., Ait-Ichou, Y., et al. Optical study of TiO2 thin films prepared by sol-gel. Ferroelectrics, 372:69e75. 2008

[75] Chakrabartty, S., Mondal, A., Sarkar, M. M., Choudhuri, B., ApuKumar Saha, A. B., & Bhattacharyya, A. TiO2 nanoparticles arrays ultraviolet-A detector with au Schottky contact. IEEE Photonics Technology Letters, 1065–1068. 2014

[76] Chinnamuthu, P., Dhar, J. C., Mondal, A., Bhattacharyya, A., & Singh, N. K. Ultraviolet detection using TiO2 nanowire array with Ag Schottky contact. Journal of Physics D: Appied Physics, 135102-01–135102-05. 2012

[77] Zhang, M., Zhang, D., Jing, F., Liu, G., Lv, K., Zhou, J., & Ruan, S. Fast decay time and low dark current mechanism in TiO2 ultraviolet detector. IEEE Photonics Technology Letters, 54–57. 2015

[78] Hazra, A., Chattopadhyay, P. P., & Bhattacharyya, P. Hybrid fabrication of highly rectifying *p-n* homojunction based on nanostructured TiO2. IEEE Electron Device Letters, 505–507. 2015

[79] Karaduman, I., Demir, M., Yildiz, E., & Acar, S. CO2 gas detection properties of a TIO2 /Al2O3 heterostructure under UV light irradiation. Physica Scripta, 055802-01–055802-08. 2015

[80] Tsai, T., Chang, S., Hsueh, T., Hsueh, H., Weng, W., Hsu, C., & Dai, B. p-Cu2 O-shell/n-TiO2 -nanowire-core heterostucture photodiodes. Nanoscale Research Letters, 1–7. 2011

[81] Zhang, M., Zhang, H., Lv, K., Chen, W., Zhou, J., Shen, L., & Ruan, S. Ultraviolet photodetector with high internal gain enhanced by TiO2 /SrTiO3 heterojunction. Optics Expers, 5936–5941. 2012

[82] Jhaveri, J., Avasthi, S., Man, G., McClain, W., Nagamatsu, K., Kahn, A., Schwartz, J., and Sturm, J. Hole Blocking Crystalline-Silicon/Titanium-Oxide Heterojunction with Very Low Interface Recombination Velocity. Physics Letters, 2013.

[83] Nabet, B. A heterojunction metal–semiconductor–metal photodetector. IEEE Photonics Technology Letters, 223–225. 1997

[84] Karaduman, I., Demir, M., Yildiz, E., & Acar, S. CO2 gas detection properties of a TIO2 /Al2O3 heterostructure under UV light irradiation. Physica Scripta, 055802-01–055802-08. 2015

[85] Tsai, T., Chang, S., Hsueh, T., Hsueh, H., Weng, W., Hsu, C., and Dai, B. p-Cu2 O-shell/n-TiO2 -nanowire-core heterostucture photodiodes. Nanoscale Research Letters, 1–7. 2011

[86] Zhang, M., Zhang, H., Lv, K., Chen, W., Zhou, J., Shen, L., & Ruan, S. Ultraviolet photodetector with high internal gain enhanced by TiO2 /SrTiO3 heterojunction. Optics Express, 5936–5941. 2012

[87] Nabet, B. A heterojunction metal–semiconductor–metal photodetector. IEEE Photonics Technology Letters, 223–225. 1997

[88] Chakrabartty, S., Mondal, A., Sarkar, M. M., Choudhuri, B., ApuKumar Saha, A. B., & Bhattacharyya, A. TiO2 nanoparticles arrays ultraviolet-A detector with au Schottky contact. IEEE Photonics Technology Letters, 1065–1068. 2014

[89] Chinnamuthu, P., Dhar, J. C., Mondal, A., Bhattacharyya, A., and Singh, N. K. Ultraviolet detection using TiO2 nanowire array with Ag Schottky contact. Journal of Physics D: Appied Physics, 135102-01–135102-05. 2012

[90] Zhang, M., Zhang, D., Jing, F., Liu, G., Lv, K., Zhou, J., & Ruan, S. Fast decay time and low dark current mechanism in TiO2 ultraviolet detector. IEEE Photonics Technology Letters, 54–57. 2015

[91] Hazra, A., Chattopadhyay, P. P., & Bhattacharyya, P. Hybrid fabrication of highly rectifying p-n homojunction based on nanostructured TiO2. IEEE Electron Device Letters, 505–507. 2015

[92] Rawat, G., Somvanshi, D., Kumar, H., Kumar, Y., Kumar C., & Jit, S. Ultraviolet detection properties of p-Si/n-TiO 2 heterojunction photodiodes grown by electron-beam evaporation and sol-gel methods: A comparative study. IEEE Transactions Nanotechnology, 193-200. 2016

[93] Dewasi, A., & Mitra, A. Effect of variation of thickness of TiO2 on the photovoltaic performance of n-TiO2/p-Si heterostructure. Journal of Materials Science: Materials in Electronics, 10854-017-7751-3. 2017

[94] Ansari, S. A., Khan, M. M., Ansari, M.O., Cho, M. H. Nitrogen-doped titanium dioxide (N-doped TiO2) for visible light photocatalysis. New Journal of Chemistry, 3000–3009. 2016

[95] https://en.wikipedia.org/wiki/Band_offset

[96] Jäger, K, Isabella, O, Smets, M, & René M., Swaaij, V, & Zeman, M Solar Energy: Fundamentals, Technology, and Systems. UIT Cambridge 2014.

[97] Luque, A, & Steven, H Handbook of photovoltaic science and engineering. (2nd ed.). A John Wiley and Sons. 2011.

[98] pn junction diode under thermal equilibrium. (n.d.). Retrieved December 26, 2018, from https://en.wikipedia.org/wiki/P–n_junction.

[99] Nasir Northern , A Power Electronics Book, Hawijah Technical Institute. 2021.

[100] http://www.osioptoelectronics.com/application-notes/AN-Photodiode Parameters Characteristics.pdf

[101] Sbeta M.N. Integration Of Sol-Gel Derived Doped Zinc Oxide Fılms And Solution-Processed Metal Nanoparticles For Thin Film Photodiode And Solar Cell Applications, Pubslished Masters, Ankara Yıldırım Beyazıt University. 2019

[102] Ahmadi, M., Wu, T., & Hu, B. A review on Organic-Inorganic Halide Perovskite Photodetectors:Device Engineering and Fundamentals Physics. Advance Materials, 29, 1605242. 2017

[103] Ni, S., Yu, Q., Huang, Y., Wang, J., Li, L., Yu, C., Guo, F., Wu, H., Lu, W., & Zhang, W. Heterostructured TiO2/MgO nanowire arrays for self-powdered UV photodetectors. RSC Advances, 6, 85951. 2016

[104] Wei, C., Xu, J., Shi, S., Cao, R., Chen, J., Dong, H., Zhang, X., Yin, S., & Li, L. Self-powdered visible-blind UV photodetectors based on p-NiO nanoflakes/n-ZnO nanorod arrays with an MgO interfacial layer. Journal of Materials Chemistry C, 7, 9369. 2019

[105] Cullity, B. D. Elements of X-Ray Diffraction (8th ed.). Addison-Wesley Publishing Company. 1978.

[106] Li, W., Liang, R., Hu A., Huang, Z. & Zhou, Y. Generation of oxygen vacancies in visible light activated one-dimensional iodine TiO2 photocatalysts. RSC Advances, 70. 2014

[107] Yuvaraja, S., Kumar, V., Dhasmana, H., & Kumar, A. Ultraviolet detection properties of electrodeposited n-SnO2 modified p-Si nanowires hetero-junction photodiode. Journal of Materials Science: Materials in Electronics, 30(8):1-1. 2019

[108] Ling, C., Guo, T., & Lu, W. Ultrahigh broadband photoresponse of SnO2 nanoparticle thin film/SiO2/p-Si heterojunction. Nanoscale Journal, 25. 2017

[109] Rasool, K., Rafiq, M. A., Ahmad, M., Imran, Z., & Hasan, M. M. TiO2 nanoparticles and silicon nanowires hybrid device: Role of interface on electrical, dielectric, and photodetection properties. Applied Physics Letters, 101, 253104. 2012

[110] Rawat, G., Somvanshi, D., Kumar, Y., Kumar, H., Kumar, C., & Jit, S. Electrical and Ultraviolet-A Detection Properties of E-Beam Evaporated n-TiO2 Capped p-Si Nanowires Heterojunction Photodiodes. IEEE Transactions on Nanotechnology, 49-57. 2017

[111] Chauhan, K., & Patel, D. Functional nanocrystalline TiO2 thin films for UV enhanced highly responsive silicon photodetectors. Journal of Alloys and Compounds, 792 968-975. 2019

[112] Sharma, S., Bayer, B.C., Skakalova, V., Singh G., & Periasamy, C. Structural, Electrical, and UV Detection Properties of ZnO/Si Heterojunction Diodes. IEEE Transactions on Electron Devices, 63,5 1949-1956. 2016

[113] Rawat, G., Somvanshi, D., Kumar, H., Kumar, Y., Kumar C., & Jit, S. Ultraviolet Detection Properties of p-Si/n-TiO_2 Heterojunction Photodiodes Grown by Electron-Beam Evaporation and Sol–Gel Methods: A Comparative Study. IEEE Transactions on Nanotechnology, 15,2 193-200. 2016

CURRICULUM VITAE

PERSONAL INFORMATION

Name Surname : Betül ŞEKERTEKİN

Date of Birth :

Phone :

E-mail :

EDUCATION

High School : Tevfik İleri Anadolu Lisesi ERZURUM

Bachelor : Metallurgical and Materials Engineering, 2018, Yıldırım Beyazıt University ANKARA

Master Degree : Energy Systems Engineering, 2022, Yıldırım Beyazıt University ANKARA

WORK EXPERIENCE

- Research and Development Engineer at Kalyon PV in Ankara. (2020-continued)
- TÜBİTAK 1001 Project, Researcher. (2018-2020)
- Intern, ARİSTON in MANİSA, (2017)
- Intern, MAGMAWELD in MANİSA, (2016)

TOPICS OF INTEREST

- Material Science
- Energy Storage
- Solar Energy

PRESENT ORGANIZED SOURCES / PRESENTATION

- 9.European Conference on Renewable Energy Systems-ECRES 2021 / Oral and Virtual Presentation
- 9.European Conference on Renewable Energy Systems-ECRES 2021 / Paper
- EU PVSEC / 2021/ Virtual Presentation and Paper
- Solar Conference Exhibition/"Examining Major Design Considerations of Solar Thermal Storage Systems" /2018/ Verbal Notice